國立交通大學

電子工程學系　電子研究所

碩士論文

梳狀引導信號輔助之多輸入輸出通道動差預估與分析

Channel Moment Estimation and Analysis for MIMO-OFDM with Comb-type Pilots

研究生：蔡咏廷

指導教授：桑梓賢　教授

中華民國九十六年六月

梳狀引導信號輔助之多輸入輸出通道動差預估與分析

Channel Moment Estimation and Analysis for MIMO-OFDM with Comb-type Pilots

研 究 生：蔡咏廷　　Student：Yung-Ting Tsai

指導教授：桑梓賢　　Advisor：Tzu-Hsien Sang

國 立 交 通 大 學

電子工程學系　電子研究所

碩 士 論 文

A Thesis

Submitted to Department of Electronics Engineering & Institute of Electronics

College of Electrical and Computer Engineering

National Chiao Tung University

in partial Fulfillment of the Requirements

for the Degree of Master

in

Electronics Engineering

August 2006

Hsinchu, Taiwan, Republic of China

中華民國九十六年六月

梳狀引導信號輔助之多輸入輸出通道動差預估與分析

研究生： 蔡咏廷　　指導教授： 桑梓賢

國立交通大學

電子工程學系　電子研究所碩士班

摘要

正交多頻分工(OFDM)系統在過去數年間已經成功的應用到許多數位通訊上。在正交分頻多工系統通道偵測上，根據梳狀引導信號(comb-type pilots)的輔助，過去已經提出了許多的方法。在這篇論文中，我們提出了一種創新的引導信號內插法(pilot interpolation)並與其他內插法比較，例如：線性內插(LI)、木條曲線內插(SCI)...。在這方法中，我們利用了通道的頻率響應(CFR)的一階與二階動差，並且時域的低通濾波器是在頻域中完成的，這意味著我們不用多一次的傅立葉轉換，因此可以省下一個快速傅立葉轉換，節省了系統的成本。另一方面，多輸入多輸出(MIMO)與正交分頻多工(OFDM)系統的結合，也就是 MIMO-OFDM，近來也是廣泛的應用在數位通訊上。因此，我們提出了一個 MIMO-OFDM 架構，可以將之前根據單輸入單輸出正交分頻多工系統(SISO-OFDM)所設計的引導信號內插演算法套用於上。

Channel Moment Estimation and Analysis in MIMO-OFDM with Comb-type Pilots Added

研 究 生：蔡咏廷　　student：*Yung-Ting Tsai*

指導教授：桑梓賢　　Advisors：*Tzu-Hsien Sang*

Department of Electronics Engineering & Institute of Electronics
National Chiao Tung University

ABSTRACT

Orthogonal frequency division multiplexing (OFDM), has been successfully applied to a wide variety of digital communications applications over the past several years. There is many channel estimation strategies are used in OFDM system with comb-type pilots inserted. This thesis introduces an innovative pilot interpolation method by using the 1st and the 2nd moments of the channel impulse response (CIR) and comparing with other methods, ex. LI, SCI ... In this innovative method, time-domain low-pass filter is implemented in frequency-domain; it means that we don't have to do another fourier transform. In this way, we can save a FFT block to reduce the system cost. On the other hand, the combinations of multi-input multi-output (MIMO) and OFDM, MIMO-OFDM, is widely applied on digital communication recently. Therefore, we introduce a MIMO-OFDM architecture that can easily apply those pilots interpolation algorithms used in single-input single-output (SISO) OFDM systems.

誌謝

在這將近三年的研究生生涯中，學習了不少研究的方法與做人處世的道理。首先要感謝指導教授桑梓賢老師，除了專業上的指導與幫助，有時更也會給我們一點思考上方向的激盪，讓我更懂得以不同的角度來看待事物。另外，非常有幸的可以到詠發科技，在李宇旼老師的身上學習到了專業與謙虛的並存，非常有耐心的指導，也對我這篇論文的生出有決定性的幫助。另外研究室的欣德學長也在有問題疑惑的時候給了我很大的幫助，同學 B 魔、阿康、Yoyo、晉運、李薇，以及各位學弟的兩年同窗生活，除了解決的研究上的問題之外，也讓我研究生涯多采多姿。最後要感謝父母親對我的支持以及栽培，還有女友容容在背後給我很大的支持及鼓勵，讓我學生生涯畫下個句點。

Contents

Chapter 1 Introduction.....1
1.1 Motivation..... 1
1.2 Introductions of Baseband OFDM Model 5
1.3 Organization of the Thesis 9
Chapter 2 Comb-type Pilot Aided Channel Estimation 10
2.1 The Signal Model of Comb-Type Pilot Channel Estimation in OFDM System.... 10
2.2 Prior Arts in One-Dimensional Interpolation Methods for Comb-Type Channel Estimation 13
2.2.1 Piecewise-Constant Interpolation 13
2.2.2 Linear Interpolation 13
2.2.3 Low-pass Interpolation 14
2.2.4 Time Domain Interpolation..... 17
2.2.5 Other Interpolation Methods.....17
2.3 Prposed Moment-Assist Low Pass Interpolation 19
2.4 The Channel Moment Estimation 22
2.4.1 How to Access the Moment of CIR.....22
2.4.2 The Discrete Form of the Moments 25
2.4.3 The Effect of Down-Sampling to the Moments Estimators.....26
2.4.4 The Relationships between Moments and Moments Estimator in Time Domain.....28
2.4.5 Improve the Accuracy of the Estimators 32
Chapter 3 Pilot-Aided Channel Estimation for MIMO-OFDM.....37
3.1 Reasons to Extend SISO-OFDM to MIMO-OFDM..... 37
3.2 The Architecture of the MIMO-OFDM 37
3.3 The Space-Time CODEC for MIMO-OFDM..... 38
3.4 How to Apply 1st and 2nd Momnets in MIMO-OFDM 40
Chapter 4 Simulation Results.....41
4.1 Some Simulation Results of the Moment Estimators 41
4.2 Some Simulation Results of the MIMO-OFDM with the Interpolation Methods . 47
Chapter 5 Conclusion 49
Reference 51

LIST OF TABLES

Table 01 Computational Complexity Analysis of Comb-Type Pilot 1-D Interpolation Methods 18
Table 02 The Encoding and Transmittion Sequence for the Two-Branch Transmit Diversity Scheme 38
Table 03 Simulations Parameters 47

LIST OF FIGURES

Fig 1.1 Two types of pilot arrangement 2
Fig 1.2 The scattered pilot arrangement 4
Fig 1.3 A basic digital implementation of a baseband OFDM system 5
Fig 2.1 Comb-Type Pilot Arrangement 11
Fig 2.2 Comb-Type Pilot Arrangement in Single OFDM Symbol 11
Fig 2.3 The Channle Estimation Block Diagram 12
Fig 2.4 Piecewise-Constant Interpolation 13
Fig 2.5 Linear Interpolation 14
Fig 2.6 The Relationships between $\hat{\mathbf{H}}0_n$ and $\mathbf{H}_n$ in Frequency Domain and Time Domian…… 18
Fig 2.7 The Low-Pass Filter that Gets the Real CIR 16
Fig 2.8 The Block Diagram of LPI 17
Fig 2.9 TDI Block Diagram 17
Fig 2.10 SER Performance versus SNR for the Channel Estimators Based on LS with Comb-Type Pilot Arrangements 18
Fig 2.11 The Example of LPI 19
Fig 2.12 A More Ideal Filter in Assumption 20
Fig 2.13 The Block Diagram of MA-LPITD 20
Fig 2.14 The Block Diagram of MA-LPIFD 21
Fig 2.15 Down Sampling Effects 27
Fig 2.16 The Summation Paths of the 1st Moment and its Estimator 30
Fig 2.17 The Summation Paths of the 2nd Moment and its Estimator 31
Fig 2.18 The Summation Paths of m1 with Down Sampling Effects 32
Fig 2.19 The Summation Paths of m2 with Down Sampling Effects 32
Fig 3.1 The Architecture of the MIMO-OFDM Channel Estimation in Current Idea . 38
Fig 3.2 The 2*M MIMO Channel Model 39
Fig 3.3 The Block Diagram of MIMO-OFDM with Alamouti Scheme 40
Fig 4.1 Three Types of PDPs 41
Fig 4.2 The Normalized MSE of m1 Estimators 43
Fig 4.3 The Normalized MSE of m2 Estimators 44

Fig 4.4 The m1 Estimator MSE of Theoretical Value and Monte Carlo Method 45
Fig 4.5 The m2 Estimator MSE of Theoretical Value and Monte Carlo Method 46
Fig 4.6 BER Performance versus SNR for the Equalizer Based On Alamouti with Comb-Type Pilot Arrangements 48

Chapter 1

Introduction

In this chapter, the motivation of the research will be described first. Then, the organization of this thesis will be presented at the end of this chapter.

1.1 Motivation

Orthogonal frequency division multiplexing (OFDM) is a multicarrier transmission technique which uses parallel data transmission and frequency division multiplexing and was drawn firstly in 1960s [1-2]. Because of its' high channel efficiency, OFDM is wildly applied in the new generation wireless access systems such as digital broadcasting systems [3]and wireless local area network [4]. On the other hand, the concept of multiple-input multiple-output (MIMO) based communications has received wide spread attention from the communication society [5]. The utilization of MIMO techniques in wireless transmission provides a tremendous increase in spectral efficiency. To achieve wideband wireless transmission at high data rate, the combination of these two techniques, MIMO-OFDM [6], is one of the best solutions to high data rate digital transmission.

In wireless communications, the receiver systems have to compensate the channel effects and the channel equalizer and channel estimation techniques are deployed. The channel equalizer recovers the original signal under non-perfect channel environment based on the estimated channel; therefore, the precision of the channel estimation is important. In general, the fading channel of OFDM systems can be viewed as a 2-dimensinal (2D) function (time and frequency) [7]. In the OFDM system with pilot added, the optimal channel estimator in terms of mean-square error is based on 2D Wiener filter interpolation.

However, the 2D wiener filter is too complex for practical implementation. Therefore, the tradeoff between complexity and performance, usually one-dimensional (1D) interpolation is adopted in OFDM systems. Basically, there are two types of 1D pilot arrangement, one is block-type pilot arrangement, and the other is comb-type pilot arrangement. And the block-type pilot arrangement and comb-type pilot arrangement are illustrated in Fig. 1.1. The block-type pilot arrangement inserts pilots in frequency direction, and its OFDM channel estimation symbols are transmitted periodically, and all subcarriers are used as pilots. On the other hand, the comb-type pilot arrangement inserts pilots in time direction, and every transmitted symbol contain pilot signals. In comb-type pilot arrangement, the pilots are uniformly inserted into the subcarriers of OFDM symbol. The latter type, comb-type pilot channel estimation, is the focus of this thesis.

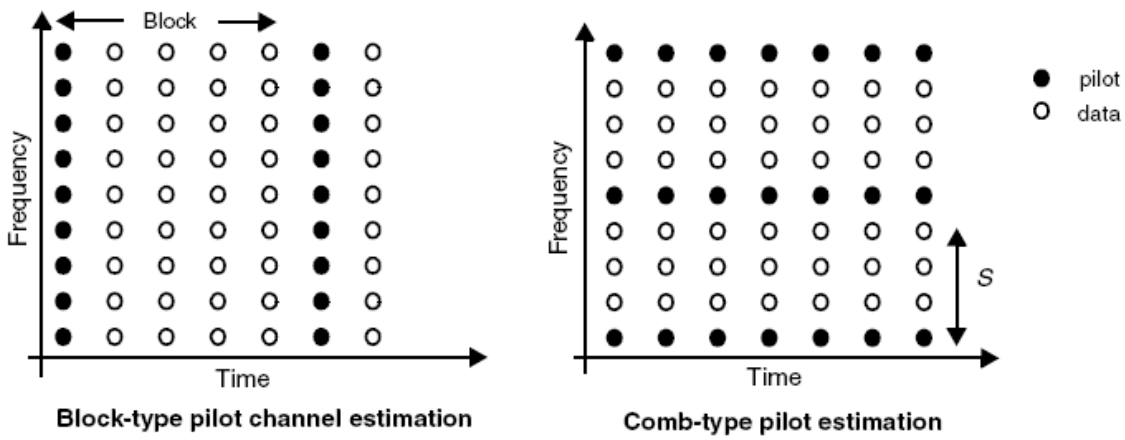

Fig 1.1 Two Types of Pilot Arrangement

In comb-type pilot arrangement, after exploiting the pilots to acquire the estimated channel frequency response (CFR) on each pilot subcarriers, there are many methods to interpolate the CFR into the data subcarriers, such as linear interpolation (LI), second-order interpolation (SOI), low-pass interpolation (LPI), and time-domain interpolation (TDI). In this thesis, we developed an innovative interpolation method that combines the ideas of time-domain/frequency-domain and low-pass filter, and uses the 1st moment and 2nd moment of the CIR to design the low-pass filter. In fact, this method can be easily

implemented if converts the estimated CFR to time domain by inverse discrete Fourier transform (IDFT). However, if there are 2K/4K/8K subcarriers, the method adding an IDFT block will cost too high to afford, such as the DVB-T/H systems. Therefore, if all the time-domain computations can be operated in frequency domain, then the method, Moments-Assisted LPI in Frequency Domain (MA-LPIFD), will be a practical one.

To do the computations in frequency domain, there are few challenges that we have to solve. First, the computations have to transform into frequency-domain by Fourier transform. Second, the first and second moments of the channel impulse response (CIR) have to be acquired in frequency domain. Third, the accuracy of MA-LPIFD needs to be further improved.

After achieving those tasks, some future works came to my mind. The first one is to adopt the pilot arrangements in DVB-T/H, the scattered pilot, Fig. 1.2 [3], then extend the 1-D channel estimation in frequency-direction to 2-D or two 1-D (2*1D) channel estimations [9]. The second one is to extend the SISO-OFDM system to MIMO-OFDM system to exploit the spatial diversity gain. In scattered pilot arrangement, the channel can be both estimated in time-direction and frequency-direction, and according to [7], 2D channel estimation yields better performance than the 1D scheme, at the expense of higher computational complexity and processing delay. However, in systems that use 2K/4K/8K modulations, if the channel has to be estimated in time-direction, we need adequate symbols to collect information in each computation, which means large amounts of memory is needed and the channel is estimated until receiving enough symbols. Therefore, comparing the first extension with the second extension, the latter one, from SISO-OFDM to MIMO-OFDM, is more interesting.

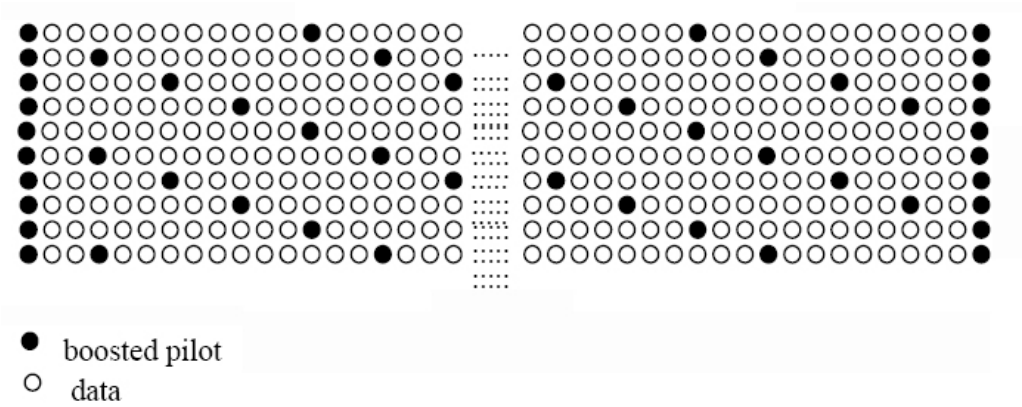

Fig. 1.2 The Scattered Pilot Arrangement

1.2 Introductions of Baseband OFDM Model

The main idea of applying OFDM systems is to split a high rate data stream into a several lower rate data streams that are transmitted simultaneously over a number of subcarriers. A basic digital implementation of a Baseband OFDM system is illustrated in Fig. 1.3.

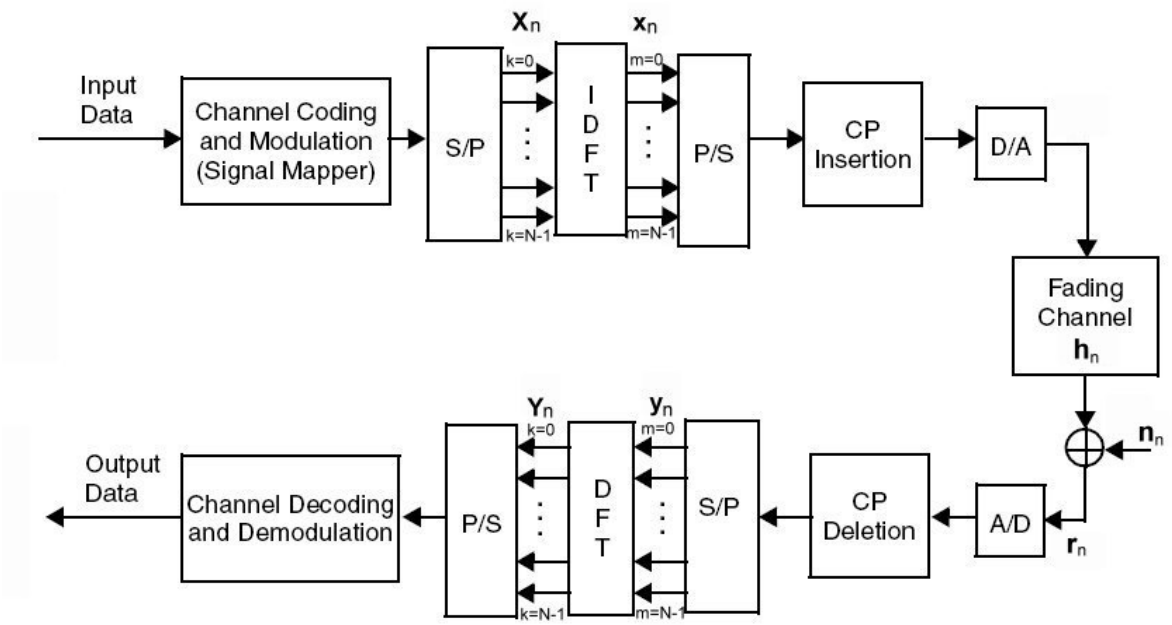

Fig. 1.3 A Basic Digital Implementation of a Baseband OFDM System

First, we have to transform the serial data stream to parallel data stream. After that, the data stream is transmitted in different subcarriers, which are divided in orthogonal frequency. An inverse discrete Fourier transform (IDFT) is used to achieve orthogonal frequency division, and the equation is shown as follows:

$$x_{[n,t]} = \tfrac{1}{N}\sum_{k=0}^{N-1} X_{[n,k]} e^{j2\pi kt/N} = \tfrac{1}{N}\sum_{k=0}^{N-1} X_{[n,k]} W_N^{-kt} \tag{1.1}$$

where N is the N-point DFT, and k represents the k-th subcarrier, and $W_N = e^{-j2\pi/N}$. $X_{[n,k]}$ represents the data in k-th subcarrier of the n-th OFDM symbol in frequency domain. $x_{[n,t]}$ represents the data in t-th section of the n-th OFDM symbol in time domain. Define that

$$\mathbf{x}_n = \left[x_{[n,0]}, \cdots, x_{[n,N-1]} \right]^{\mathrm{T}}$$
$$\mathbf{X}_n = \left[X_{[n,0]}, \cdots, X_{[n,N-1]} \right]^{\mathrm{T}}. \tag{1.2}$$

Following the IDFT block and parallel-to-serial (P/S) block, the cyclic prefix block (CP) extends the time length T_G, which is larger than the expected delay spread. In discrete computation, the extended length is larger than the channel path number.

The digital-to-analog converter (DAC) contains low-pass filter with bandwidth 1/Ts, where Ts is the sampling interval. In the discrete form, the mathematical expression of this block is not shown.

The channel is modeled as a sampled impulse response. Denote $h_{[n,l]}$ and $n_{[n,l]}$ as the l-th coefficient of the channel impulse response and complex additive white Gaussian noise (AWGN) at the n-th OFDM block respectively. From the discrete Fourier transform, the CFR and noise frequency response are defined as

$$H_{[n,k]} = \sum_{l=0}^{L-1} h_{[n,l]} W_N^{kl}$$
$$N_{[n,k]} = \sum_{l=0}^{L-1} n_{[n,l]} W_N^{kl} \tag{1.3}$$

where $H_{[n,k]}$ and $N_{[n,k]}$ represent the CFR and noise frequency response at the k-subcarrier of the n-th OFDM block respectively. Denote that L is the known maximum channel length, $W_N = e^{-j2\pi/N}$ and N is the OFDM block size and L<N is assumed [8]. And we defined that

$$\mathbf{h}_n = \left[h_{[n,0]}, \cdots, h_{[n,L-1]} \right]^{\mathrm{T}}$$
$$\mathbf{H}_n = \left[H_{[n,0]}, \cdots, H_{[n,N-1]} \right]^{\mathrm{T}} \tag{1.4}$$

are CIR and CFR vectors of n-th OFDM symbol respectively. And

$$\mathbf{n}_n = \left[n_{[n,0]}, \cdots, n_{[n,L-1]} \right]^{\mathrm{T}}$$
$$\mathbf{N}_n = \left[N_{[n,0]}, \cdots, N_{[n,N-1]} \right]^{\mathrm{T}} \tag{1.5}$$

are noise impulse response and noise frequency response vectors of n-th OFDM symbol respectively.

And the CIR $\mathbf{h}_n$ and CFR $\mathbf{H}_n$ has the following relationship

$$\mathbf{H}_n = \mathbb{F}\mathbf{h}_n . \tag{1.6}$$

So as for $\mathbf{n}_n$ and $\mathbf{N}_n$,

$$\mathbf{N}_n = \mathbb{F}\mathbf{n}_n \tag{1.7}$$

where

$$\mathbb{F} = \begin{bmatrix} W_N^0 & W_N^0 & \cdots & W_N^0 \\ W_N^0 & W_N^1 & \cdots & W_N^{L-1} \\ \vdots & \vdots & \ddots & \vdots \\ W_N^0 & W_N^{L-1} & \cdots & W_N^{(N-1)(L-1)} \end{bmatrix}.$$

At the receiver, after passing through the analog-to-digital converter (ADC) and removing the CP, the S/P block transforms the serial data stream into parallel, and the DFT block transfers the time domain data to frequency domain data. Define that

$$\mathbf{y}_n = \left[y_{[n,0]}, \cdots, y_{[n,N-1]} \right]^{\mathrm{T}}$$
$$\mathbf{Y}_n = \left[Y_{[n,0]}, \cdots, Y_{[n,N-1]} \right]^{\mathrm{T}} \tag{1.8}$$

where $Y_{[n,k]}$ represents the received data in k-th subcarrier of the n-th OFDM symbol in frequency domain, and $y_{[n,t]}$ represents the received data in t-th section of the n-th OFDM symbol in time domain. And $\mathbf{Y}_n$ and $\mathbf{y}_n$ are the vectors of n-th OFDM received symbol. And as same as transmitted signals, the received signals have following relationship, $Y_{[n,k]}$ =DFT($y_{[n,t]}$).

Under the assumption that the interferences are totally removed [10], the system can

be expressed as follow

$$\mathbf{Y}_n = \mathbf{H}_n \bar{\mathbf{X}}_n + \mathbf{N}_n \tag{1.9}$$

Where

$$\bar{\mathbf{X}}_n = \begin{bmatrix} X_{[n,0]} & 0 & \cdots & 0 \\ 0 & X_{[n,1]} & \ddots & \vdots \\ \vdots & \ddots & \ddots & 0 \\ 0 & \cdots & 0 & X_{[n,N-1]} \end{bmatrix}$$

In channel estimation, the transmitted signals and received signals are assumed known. Based on (1.9), the channel can be estimated by, for instance, the least square estimator (LS) or the minimum mean square error (MMSE) estimator, and these estimated CFR are expressed as follow

$$\hat{\mathbf{H}}_{n,\mathrm{LS}} = \left(\bar{\mathbf{X}}_n\right)^{-1} \mathbf{Y}_n = \left[Y_{[n,0]} / X_{[n,0]}, \cdots, Y_{[n,N-1]} / X_{[n,N-1]} \right]^{\mathrm{T}} \tag{1.10}$$

$$\hat{\mathbf{H}}_{n,\mathrm{MMSE}} = \mathbf{R}_{n,\mathbf{HH}} \left[\mathbf{R}_{n,\mathbf{HH}} + \sigma_{n,N}^2 \left(\bar{\mathbf{X}}_n \bar{\mathbf{X}}_n\right)^{-1} \right]^{-1} \hat{\mathbf{H}}_{n,\mathrm{LS}} \tag{1.11}$$

where

$$\mathbf{R}_{n,\mathbf{HH}} = E\left\{ \left(\mathbb{F}\mathbf{h}_n\right)\left(\mathbb{F}\mathbf{h}_n\right)^{\mathrm{H}} \right\} = \mathbb{F}\mathbf{R}_{n,\mathbf{hh}}\mathbb{F}^{\mathrm{H}}$$

$$\sigma_{n,N}^2 = E\left\{ \left|\mathbf{N}_n\right|^2 \right\}$$

After accessing the estimated CIR (1.10) or (1.11), for comb-type pilot arrangement, the estimated CFR on pilot subcarriers is used to interpolate the unknown CFR on data subcarriers to reconstruct the entire CFR on all subcarriers. Since the CFR is acquired, based on (1.9), the transmitted signal $\bar{\mathbf{X}}_n$ can be calculated by some equalizer, such as zeros-forcing equalizer (ZF).

1.3 Organization of the Thesis

The organization of this thesis is as follow. In Chapter 2, some comb-type pilot interpolation methods will be introduced, after that, we will discuss our interpolation method in detail. In Chapter 3, the architecture of MIMO-OFDM that adopts the interpolation method we bring out will be introduced. In Chapter 4, we will show the simulations results and analysis of these methods. At last, the conclusion and future works will be discussed in Chapter 5.

Chapter 2

Comb-Type Pilot Aided Channel Estimation

2.1 The Signal Model of Comb-Type Pilot Channel Estimation in OFDM System

OFDM is becoming widely applied in digital wireless communication systems due to its high data rate and high bandwidth efficiency. For wideband mobile communication system, the channel between transmitter and receiver is usually frequency-selective and time-variant. However, most channel estimation methods for OFDM system are developed under the assumption that the channel is stationary within one packet, and those methods are not suitable under mobile communication channel. Therefore, a dynamic channel estimation method for frequency-selective and time variant channel is needed. The pilot-based channel estimation has been proven suitable for OFDM systems in mobile communication channels [7].

In comb-type pilot arrangement, as shown in Fig. 2.1, for each transmitted symbol, N_p pilots signals are uniformly inserted into N subcarriers in $\mathbf{X}_n$. F_S is the distance of two pilots subcarriers, where F_S=N/ N_p. In Fig. 2.2, a more detail com-type pilot arrangement in single OFDM symbol is illustrated.

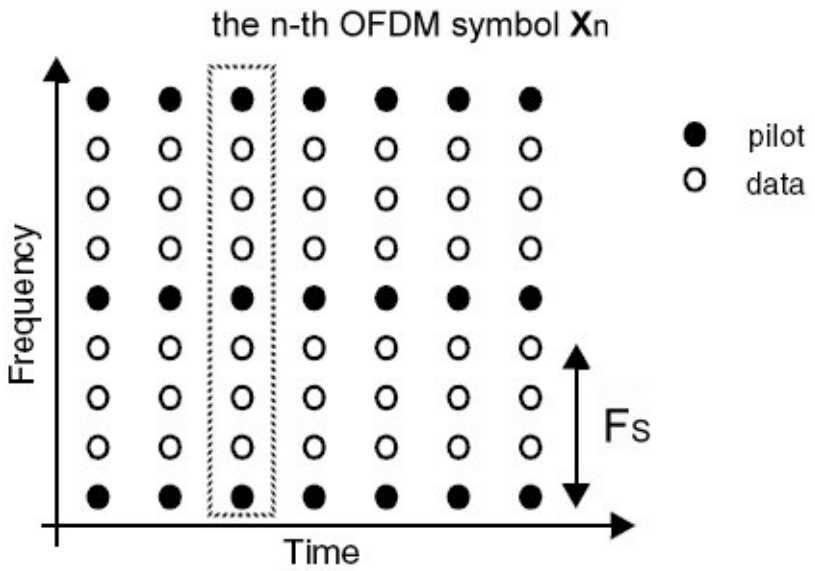

Fig. 2.1 Comb-Type Pilot Arrangement

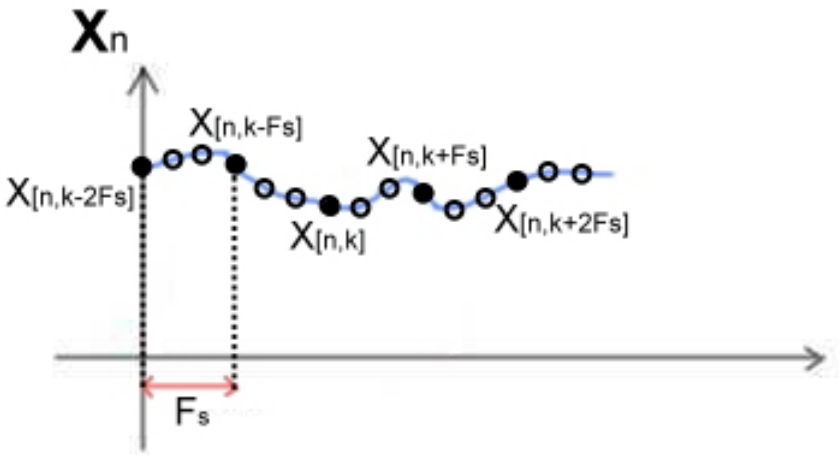

Fig. 2.2 Comb-type Pilot Arrangement in Single OFDM Symbol

Denote that the subcarrier address of pilots in each OFDM symbol is the same, and can be expressed as follow

$$\mathbf{p} = \left[p(0), p(1), \cdots, p\left(N_p - 1\right) \right]^{\mathrm{T}}, p(k) = (k-1) F_s \quad \mathrm{k} = 1 \sim N_p \tag{2.1}$$

and the pilot values are

$$\mathbf{X}^{\mathrm{P}} = \left[X^{\mathrm{P}(0)}, X^{\mathrm{P}(1)}, \cdots, X^{\mathrm{P}(\mathrm{N_p}-1)} \right]^{\mathrm{T}}. \tag{2.2}$$

At the receiver, if pilot values and subcarrier address are known, then CFR at the pilot subcarrier can be calculated by some method, for example, LS estimator, equation 1.10, or

some other algorithms. Denote that the estimated CFR at the pilot subcarriers of n-th OFDM symbol as follow

$$\hat{\mathbf{H}}_n^{\mathrm{P}} = \left[\hat{H}_n^{\mathrm{P}(0)}, \hat{H}_n^{\mathrm{P}(1)}, \cdots, \hat{H}_n^{\mathrm{P}(\mathrm{N_p}-1)} \right]^{\mathrm{T}} \tag{2.3}$$

where $\hat{H}_n^{\mathrm{P}(0)} = \hat{H}_{[n,\mathrm{P}(0)]}$. Since estimated CFR at the pilot subcarrier are acquired, there are some interpolation methods to interpolate the CFR between two pilot subcarriers. The channel estimation block diagram is shown as Fig. 2.3.

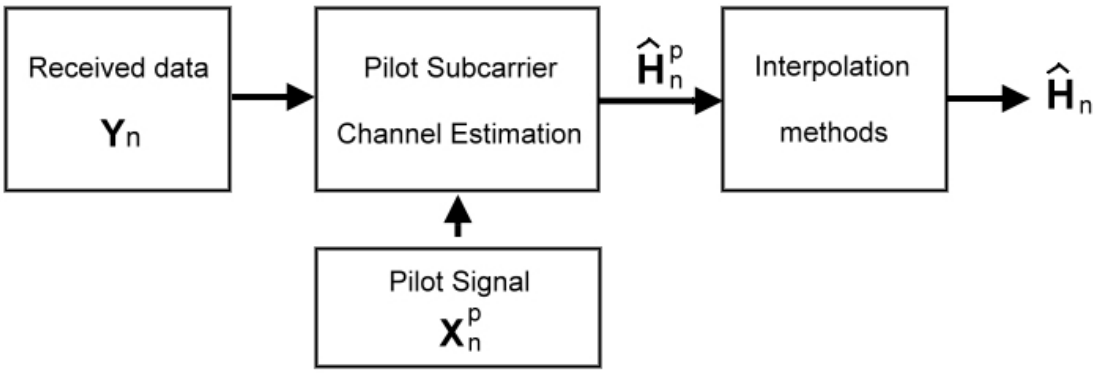

Fig. 2.3 The Channel Estimation Block Diagram

2.2 Prior Arts in One-Dimensional(1-D) Interpolation Methods for Comb-type Channel Estimation

One-dimensional interpolation is used to estimate the CFR at the data subcarriers, with reference to the estimated CFR at the pilot subcarriers, and some methods are summarized in the following section [7].

2.2.1 Piecewise-Constant Interpolation

The piecewise interpolation is the simplest interpolation method. With mathematical expression, the data subcarrier CFR between two pilot subcarrier $\hat{H}_n^{P(k)}$ and $\hat{H}_n^{P(k+1)}$ are estimated as follow, and illustrated in Fig. 2.4.

$$\hat{H}_n^{P(k)+i} = \hat{H}_n^{P(k)} \quad \text{,where } i=1 \sim F_S - 1 \tag{2.4}$$

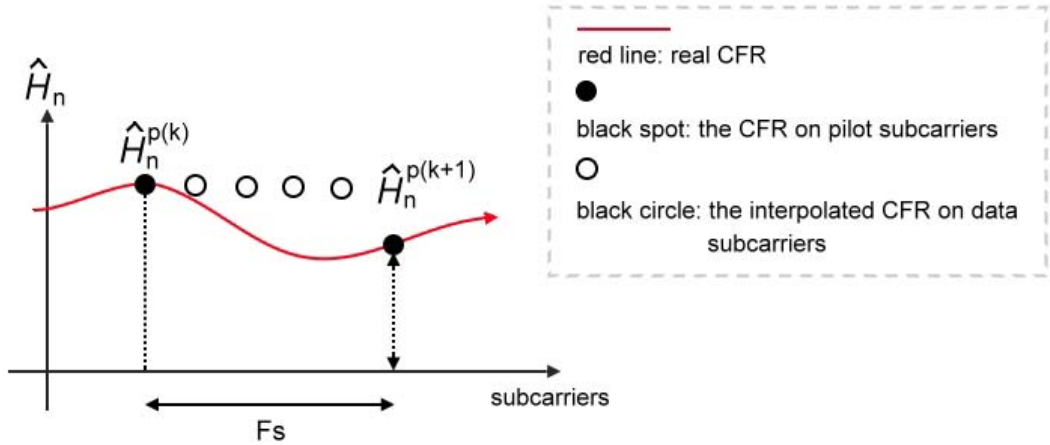

Fig. 2.4 Piecewise-Constant Interpolation

2.2.2 Linear Interpolation (LI)

The LI interpolation method performs better than piecewise-constant interpolation, and the data subcarrier CFR between two pilot subcarrier $\hat{H}_n^{P(k)}$ and $\hat{H}_n^{P(k+1)}$ are estimated as follow equation, and illustrated in Fig. 2.5.

$$\hat{H}_{[n,\mathrm{P}(k)+i]} = \hat{H}_n^{\mathrm{P}(k)} + i \times \frac{\hat{H}_n^{\mathrm{P}(k+1)} - \hat{H}_n^{\mathrm{P}(k)}}{F_S} \qquad \text{,where } i=1 \sim F_S - 1 \tag{2.5}$$

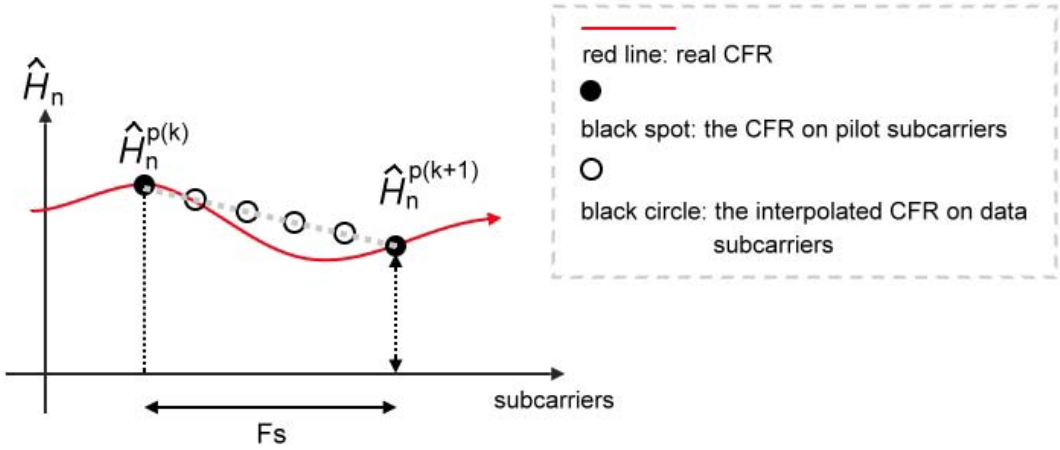

Fig. 2.5 Linear Interpolation

2.2.3 Low-pass Interpolation(LPI)

The LPI method is performed by inserting zeros in to $\hat{\mathbf{H}}_n^{\mathrm{P}}$, and then applying a low-pass finite-length impulse response (FIR) filter. The data in pilot subcarriers is not changed, and the data in the data subcarriers will be interpolated.

This method minimized the mean-square error between real value and interpolated value [7]. The idea of this method is also the inspiration of our algorithms. To explain this method, we need to figure out what padding zeros and low-pass filtering do in both time domain and frequency domain. Assumed that the estimated CFR on pilot subcarrier are equal to the real CFR, that is

$$\hat{\mathbf{H}}_n^{\mathrm{P}} = \left[\hat{H}_n^{\mathrm{P}(0)}, \hat{H}_n^{\mathrm{P}(1)}, \cdots, \hat{H}_n^{\mathrm{P}(\mathrm{N_p}-1)}\right]^{\mathrm{T}} = \mathbf{H}_n^{\mathrm{P}} = \left[H_n^{\mathrm{P}(0)}, H_n^{\mathrm{P}(1)}, \cdots, H_n^{\mathrm{P}(\mathrm{N_p}-1)}\right]^{\mathrm{T}},$$

assume that the channel path is L, and then do N-points DFT to transform to frequency domain. After padding F_S-1 zeros into $\hat{\mathbf{H}}_n^{\mathrm{P}}$, it becomes

$$\hat{\mathbf{H}}0_n = \left[\hat{H}_n^{\mathrm{P}(0)}, \underbrace{0, \cdots, 0}_{F_S-1 \text{ zeros}}, \hat{H}_n^{\mathrm{P}(1)}, 0, \cdots, 0, \hat{H}_n^{\mathrm{P}(\mathrm{N_p}-1)}\right]^{\mathrm{T}} \tag{2.6}$$

It is assumed that $N/F_S>L$, which means no aliasing at time domain. And denote

$$\begin{aligned}\hat{\mathbf{h}}0_n &= \mathrm{IDFT}\left(\hat{\mathbf{H}}0_n\right)\\ \mathbf{h}_n &= \mathrm{IDFT}\left(\mathbf{H}_n\right)\end{aligned}. \tag{2.7}$$

The relationship between $\hat{\mathbf{H}}0_n$ and $\mathbf{H}_n$ in frequency domain and time domain is shown in Fig. 2.6, and the elements of $\hat{\mathbf{H}}0_n$ and $\mathbf{H}_n$ can be expressed as following equation

$$\hat{H}0_{[n,k]} = \frac{H_{[n,k]}\sum_{i=0}^{F_S-1} e^{j\frac{2\pi ki}{F_S}}}{F_S} \tag{2.8}$$

We can see that, after padding zeros in $\hat{\mathbf{H}}_n^{\mathrm{P}}$, the impulse response of $\hat{\mathbf{H}}0_n$, $\hat{\mathbf{h}}0_n$, is F_S times repetitions of $\mathbf{h}_n$ and $1/F_S$ of its amplitude. Therefore, a low pass filter is used to pass through $\hat{\mathbf{h}}0_n$ is needed to get one copy of the repetition CIR. Theoretically, the width of this filter is 2*N/FS, which is shown in Fig. 2.7. The time domain low-pass filter can be implemented by a finite length impulse (FIR) response filter, and applied after $\hat{\mathbf{H}}0_n$, Fig. 2.8 shows the block diagram of LPI..

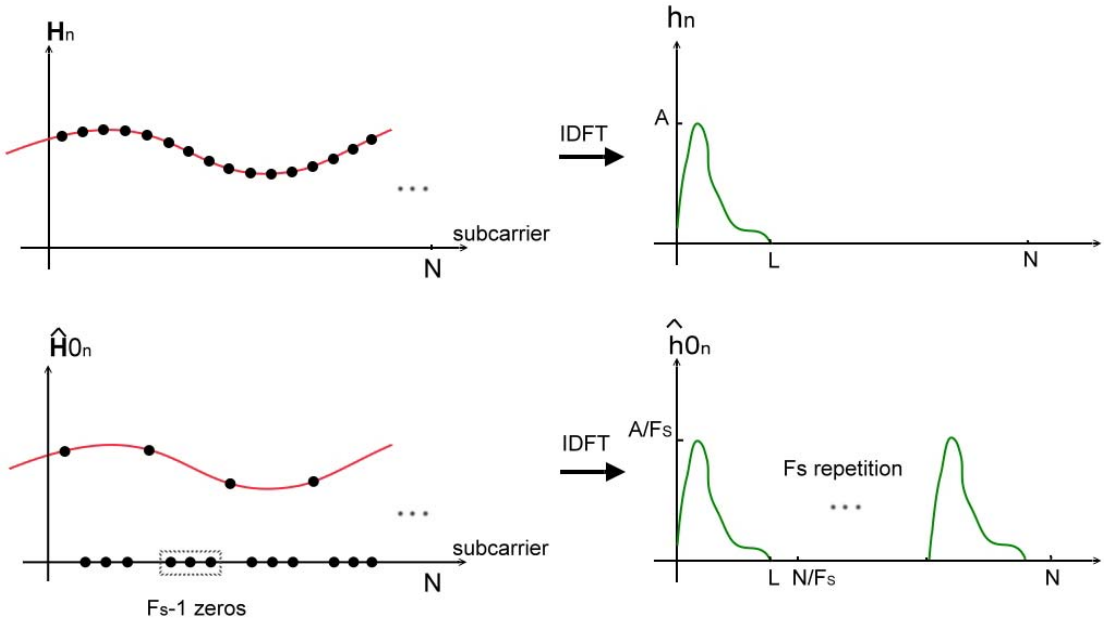

Fig. 2.6 The Relationships Between $\hat{H}0_n$ and H_n in Frequency Domain and Time Domain

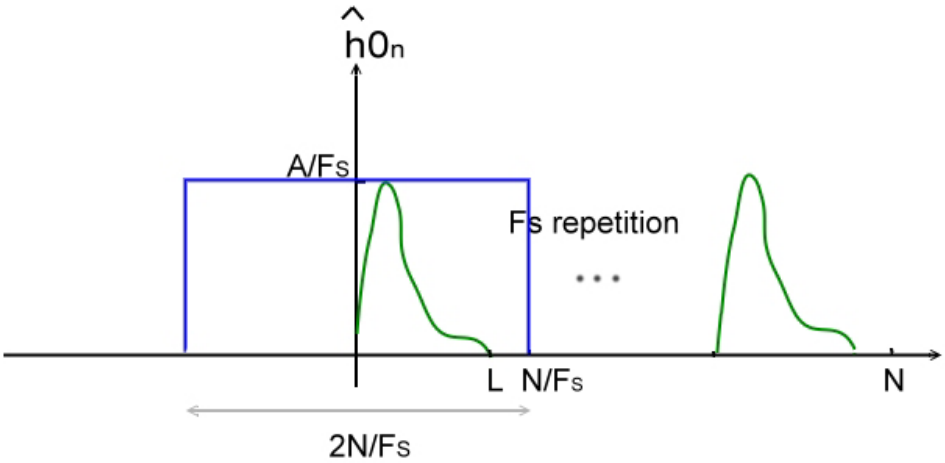

Fig. 2.7 The Low-Pass Filter that Gets The Real CIR

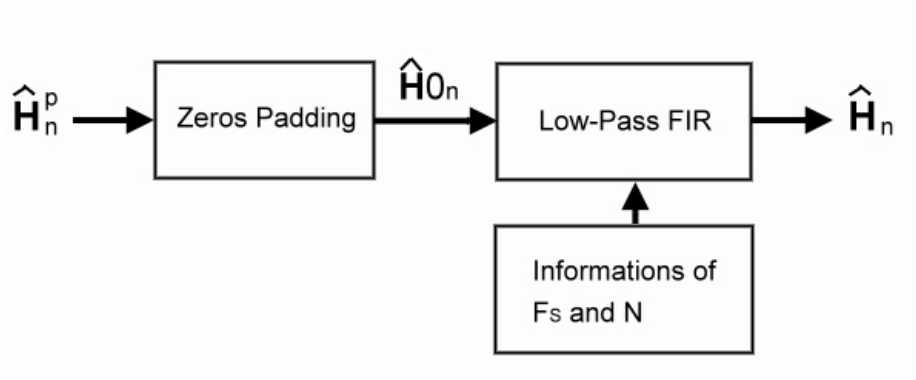

Fig. 2.8 The Block Diagram of LPI

2.2.4 Time Domain Interpolation (TDI)

The TDI method is a high-resolution interpolation based on DFT/IDFT. It first converts $\hat{\mathbf{H}}_n^P$ to time domain by IDFT, and then interpolate the time domain data to N-points by piecewise-constant interpolation or linear interpolation method. The block diagram of TDI is shown in Fig. 2.9.

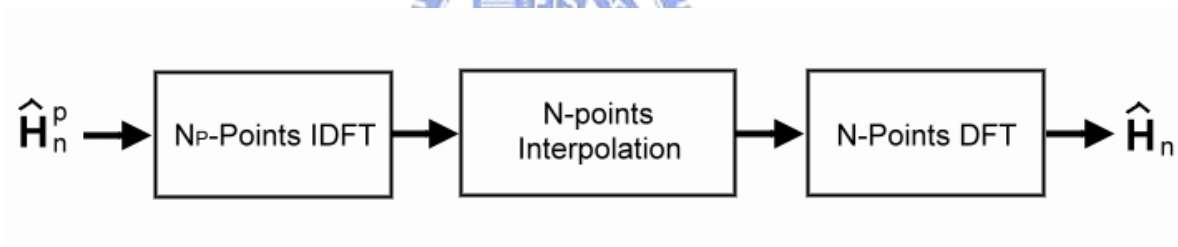

Fig. 2.9 TDI Block Diagram

2.2.5 Other Interpolation Methods

Besides the methods we introduced in 2.2.1 to 2.2.4, there are other 1-D interpolation methods, for example, Second-Order Interpolation (SOI) and Spline Cubic Interpolation (SCI) which exploit three adjacent pilot data and continuous polynomial fitting to estimate CFR respectively. The complexity analysis and simulation performance are shown in Table1 and Fig. 2.10 [7].

Estimation Scheme	Complexity	Comments
PCI	Lowest	Simple estimation and interpolation methods
LI	Lowest	
SOI	Low	
SCI	Moderated	Interpolation methods are relatively complex, with fitted polynomial, low-pass convolution, and DFT/IDFT calculation, respectively
LPI		
TDI		

Table 1: Computational Complexity Analysis of Comb-Type Pilot 1-D Interpolation Methods

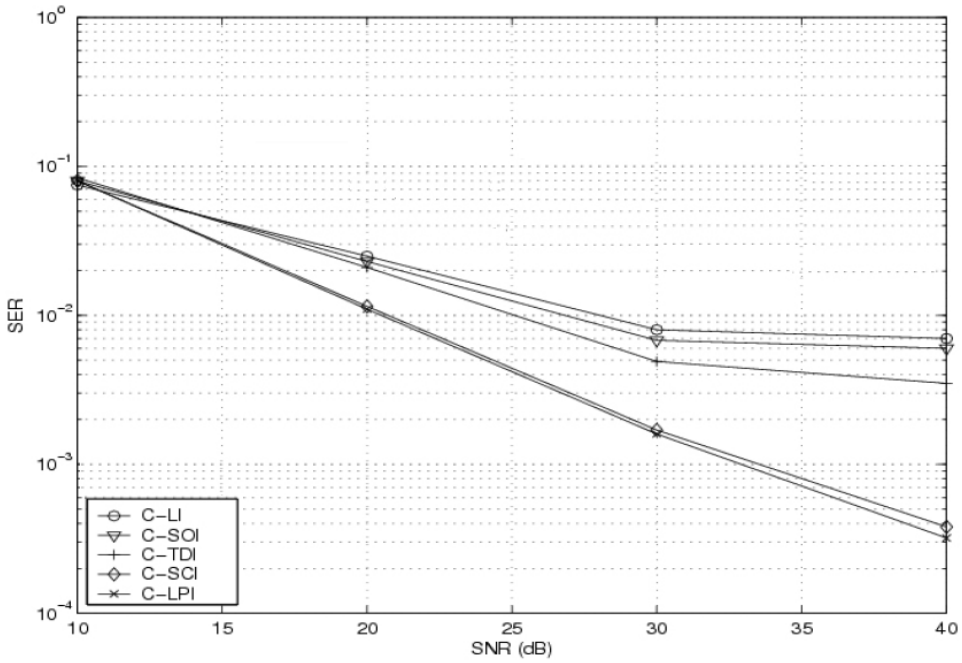

Fig. 2.10 SER Performance versus SNR for the Channel Estimators Based on LS with Comb-Type Pilot Arrangements

2.3 Proposed Moments-Assisted Low Pass Interpolation (MA-LPI)

In those 1-D interpolation methods, with mathematical analysis and simulation results, LPI method is the best performance. In LPI method, the width of low-pass FIR filter is decided by N-points FFT and the distance between two pilot subcarriers. However, there are still some places that can be improved. For example, in 2K-points FFT system, the distance of two pilot subcarriers is 4 (F_S=4), and the channel length L is 40. In LPI method, the width of low-pass filter will be 2K/4, which is much longer than the channel length L, and a lot noise (AWGN noise, the red part) will be filtered in. This example is shown in Fig. 2.11; we can see that, a lot of undesired noises (the red part) are passed by the wide width low-pass filter. If the filter width can be tuned to get lesser noise, the signal to noise ratio (SNR) will be raised, and the SER/BER will be lowered. In Fig. 2.12, a more ideal filter in assumption is shown. Therefore, the idea is that if the range can be tuned with respect to the CFR or CIR, the new filter will be more ideal [11].

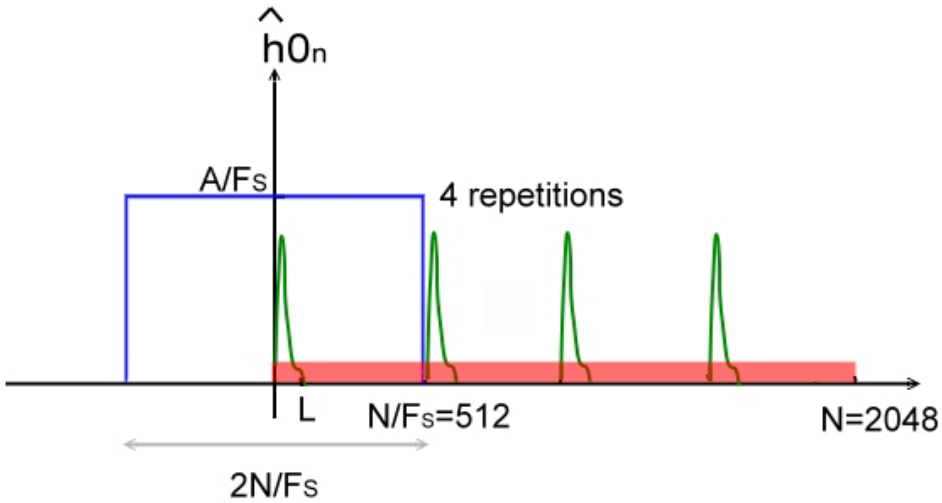

Fig. 2.11 The Example of LPI

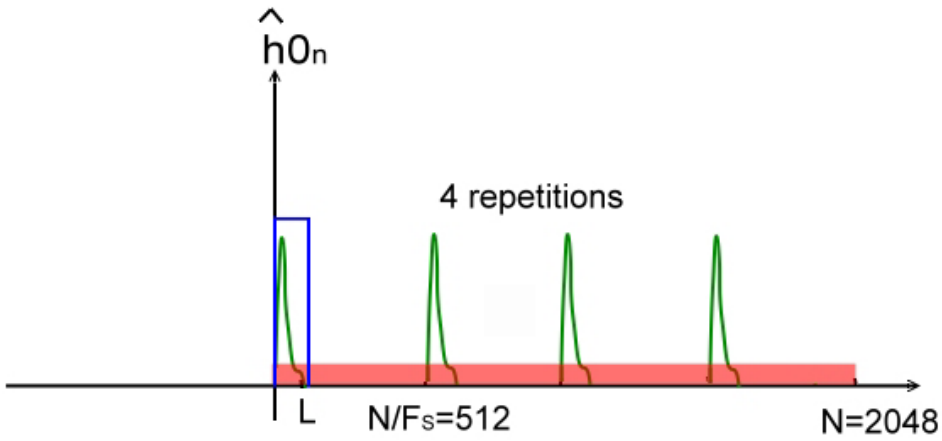

Fig. 2.12 A more Ideal Filter in Assumption

A bigger question is how to exploit the CIR/CFR information to design the filter. There are two parameters we eager to know, the first one is where the center of the CIR is, and the second one, what's the length of the CIR is. If the CIR is acquired, these two parameters can be accessed easily. The center of the CIR can be accessed by setting the threshold of the amplitude of CIR, and then find out the center and the width of this band-pass filter. Of course, it needs DFT/IDFT blocks to transform $\hat{\mathbf{H}}_n^{\mathrm{P}}$ to time domain. This idea, is rather similar to the combination of LPI and TDI, however, this is the first version of this interpolation method. The only drawback of this idea is the high cost of IDFT/DFT block. The block diagram of the current idea, called Parameters-Assisted Low Pass Interpolation in Time Domain (PA-LPITD), is shown in Fig. 2.13.

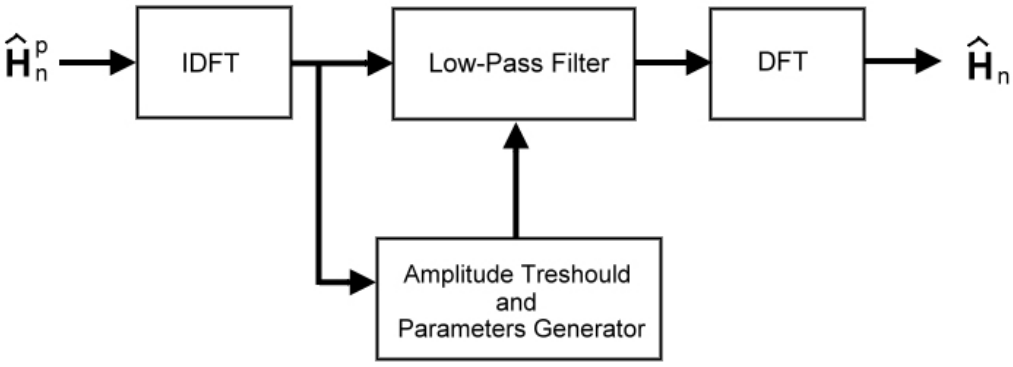

Fig. 2.13 The Block Diagram of PA-LPITD

Since the IDFT/DFT blocks cost too high, the target to improve this algorithm is to

access the filter parameters in frequency domain. In this way, all the computation is completed in frequency domain, and the IDFT/DFT blocks are negligible. However, the center and the length of the CIR are not accessible in frequency domain, but the centroid (the first moment) and the second moment of CIR are accessible in frequency domain. Therefore, in the second version algorithm, the center of the CIR is replaced by the first moment of CIR, the length of CIR is replaced by the second centre moment of CIR, and the IDFT/DFT blocks are removed. This method, which is called Moments-Assisted Low Pass Interpolation in Frequency Domain (MA-LPIFD), accesses these parameters in frequency domain, and it is discussed in *Chapter 2.4*. In Fig. 2.14, the block diagram of MA-LPIFD is shown.

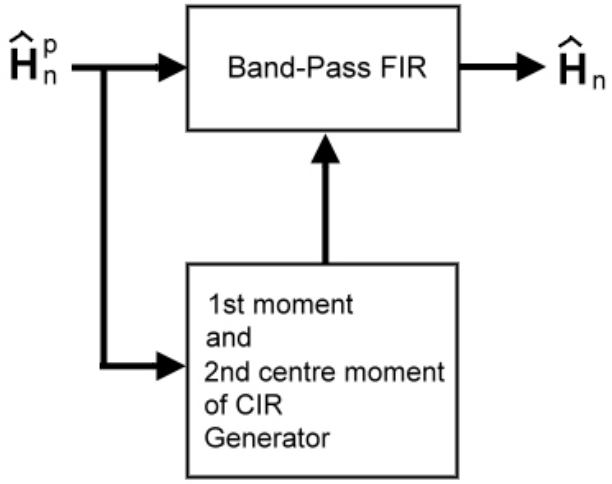

Fig. 2.14 The Block Diagram of MA-LPIFD

2.4 The Channel Moment Estimation

In this section, we will focus on the estimation of the 1st moment and 2nd centre moments of CIR. In section 2.4.1, it will be discussed in continuous time, to figure out the method to access moments in frequency domain. In section 2.4.2, the discrete form of the moment estimators will be shown. In section 2.4.3, the down sampling effects will be discussed. In section 2.4.4, the relationships between moments and moments estimators are discussed, and some improvements of the estimators are also introduced in section 2.4.5. Some simulation of this improvement is shown in section 2.4.6.

2.4.1 How to Access the Moments of CIR

Denote that the continuous time CIR is $h(t)$, and $h_0(t) = |h(t)|^2$ is the square of absolute of $h(t)$ in continuous time.

Because the CIR is complex number, the square of absolute value of CIR is used in following calculation. Of course, there are some differences between $h(t)$ and $|h(t)|^2$, but not much differences in the moments calculations. To design the filter, the following information of $|h(t)|^2$ is required: the 1st moment m_1, the 2nd centre moment $m_{2,centre}$ and the 2nd moment m_2 . They are shown in the following equations:

$$m_1 = \frac{\int t\,|h(t)|^2\,dt}{\int |h(t)|^2\,dt} \tag{2.9}$$

$$m_{2,centre} = \frac{\int t^2\,|h(t-m_1)|^2\,dt}{\int |h(t-m_1)|^2\,dt} = \frac{\int t^2\,|h_1(t)|^2\,dt}{\int |h_1(t)|^2\,dt} \tag{2.10}$$

$$m_2 = \frac{\int t^2\,|h(t)|^2\,dt}{\int |h(t)|^2\,dt} \tag{2.11}$$

denote that $h_1(t) = h(t-m_1)$. Since all the calculations are completed in frequency domain,

and (2.9), (2.10), (2.11) are functions of continuous time. These functions need a bridge to connect frequency domain and time domain, and the Fourier transform is the one to connect two different domains. The Fourier transforms of $\left|h(t)\right|^2$ and $\left|h_1(t)\right|^2$ are shown in (2.12a) and (2.12b) respectively. (2.13) is the differential of (2.12) to frequency; (2.14) is the second differential of (2.12) to frequency.

$$F\left\{\left|h(t)\right|^2\right\} = R_{HH}(f) = \int_{-\infty}^{\infty}\left|h(t)\right|^2 e^{-j2\pi ft}dt \tag{2.12a}$$

$$F\left\{\left|h_1(t)\right|^2\right\} = R_{HH1}(f) = \int_{-\infty}^{\infty}\left|h_1(t)\right|^2 e^{-j2\pi ft}dt \tag{2.12b}$$

$$R_{HH}'(f) = \frac{dR_{HH}(f)}{df} = \int_{-\infty}^{\infty} -j2\pi t\left|h(t)\right|^2 e^{-j2\pi ft}dt \tag{2.13a}$$

$$R_{HH1}'(f) = \frac{dR_{HH1}(f)}{df} = \int_{-\infty}^{\infty} -j2\pi t\left|h_1(t)\right|^2 e^{-j2\pi ft}dt \tag{2.13b}$$

$$R_{HH}''(f) = \frac{d^2R_{HH}(f)}{df^2} = \int_{-\infty}^{\infty} (-j2\pi t)^2\left|h(t)\right|^2 e^{-j2\pi ft}dt \tag{2.14a}$$

$$R_{HH1}''(f) = \frac{d^2R_{HH1}(f)}{df^2} = \int_{-\infty}^{\infty} (-j2\pi t)^2\left|h_1(t)\right|^2 e^{-j2\pi ft}dt \tag{2.14b}$$

And if f=0, (2.12a), (2.13), (2.14) can be written as follows:

$$R_{HH}(0) = \int_{-\infty}^{\infty}\left|h(t)\right|^2 dt \tag{2.15}$$

$$\left.\frac{R_{HH}'(f)}{-j2\pi}\right|_{f=0} = \frac{R_{HH}'(0)}{-j2\pi} = \int_{-\infty}^{\infty} t\left|h(t)\right|^2 dt \tag{2.16a}$$

$$\left.\frac{R_{HH1}'(f)}{-j2\pi}\right|_{f=0} = \frac{R_{HH1}'(0)}{-j2\pi} = \int_{-\infty}^{\infty} t\left|h_1(t)\right|^2 dt \tag{2.16b}$$

$$\left.\frac{R_{HH}'(f)}{(-j2\pi)^2}\right|_{f=0} = \frac{R_{HH}''(0)}{-4\pi^2} = \int_{-\infty}^{\infty} t^2\left|h(t)\right|^2 dt \tag{2.17a}$$

$$\left.\frac{R_{HH1}'(f)}{(-j2\pi)^2}\right|_{f=0} = \frac{R_{HH1}''(0)}{-4\pi^2} = \int_{-\infty}^{\infty} t^2\left|h_1(t)\right|^2 dt \tag{2.17b}$$

where $R_{HH}(f) = \int_{-\infty}^{\infty} H^*(\tau)H(f+\tau)d\tau$ is the autocorrelation of CFR. From (2.15) and (2.16a), the first moment can be expressed in frequency domain:

$$m_1 = \frac{R_{HH}'(0)}{-j2\pi \times R_{HH}(0)}. \tag{2.18}$$

And the differential functions can express as follows:

$$m_1 = \lim_{\Delta f \to 0} \left. \frac{R_{HH}(f+\Delta f) - R_{HH}(f-\Delta f)}{2\Delta f} \right|_{f=0} \Big/ -j2\pi R_{HH}(0) \tag{2.19}$$

And the approximate of (2.19) is

$$\begin{aligned} \hat{m}_1 &\approx \frac{R_{HH}(\Delta f) - R_{HH}(-\Delta f)}{2\Delta f} \Big/ -j2\pi R_{HH}(0) \\ &\overset{\Delta f = F}{=} \frac{R_{HH}(F) - R_{HH}(-F)}{2F} \Big/ -j2\pi R_{HH}(0) \end{aligned} \tag{2.20}$$

where F is division between two subcarrier frequencies. Since $R_{HH}(f)$ and $R_{HH}(-f)$ are complex conjugate, (2.20) can rewrite as

$$\hat{m}_1 = \frac{2\,\mathrm{Im}\{R_{HH}(F)\}}{-2F\,2\pi R_{HH}(0)} = -\frac{\mathrm{Im}\{R_{HH}(F)\}}{2\pi F R_{HH}(0)}. \tag{2.21}$$

From (2.15) and (2.17a), the 2nd moment is written as

$$m_2 = \frac{R_{HH}''(0)}{-4\pi^2 \times R_{HH}(0)}. \tag{2.22}$$

From (2.15) and (2.17b), the 2nd centre moment is written as

$$m_{2,centre} = \frac{R_{HH1}''(0)}{-4\pi^2 \times R_{HH1}(0)}. \tag{2.23}$$

And the approximation of (2.22) is

$$\begin{aligned} \hat{m}_2 &\approx \left. \frac{R_{HH}'(f+\Delta f) - R_{HH}'(f-\Delta f)}{2\Delta f} \right|_{f=0} \Big/ -4\pi^2 R_{HH}(0). \\ &\overset{\Delta f = \frac{F}{2}}{=} R_{HH}'(\tfrac{F}{2}) - R_{HH}'(-\tfrac{F}{2}) \Big/ -4\pi^2 R_{HH}(0) F \end{aligned} \tag{2.24}$$

And the upper part of (2.24) can express as follows:

$$\because R_{HH}{}'(f) = \frac{R_{HH}(f+\Delta f) - R_{HH}(f-\Delta f)}{2\Delta f}$$

$$\therefore R_{HH}{}'(\tfrac{F}{2}) = \left.\frac{R_{HH}(f+\Delta f) - R_{HH}(f-\Delta f)}{2\Delta f}\right|_{f=\frac{F}{2}}$$

$$R_{HH}{}'(-\tfrac{F}{2}) = \left.\frac{R_{HH}(f+\Delta f) - R_{HH}(f-\Delta f)}{2\Delta f}\right|_{f=-\frac{F}{2}}$$

(2.24) can rewrite as follows:

$$\begin{aligned}
\hat{m}_2 &= \left(\frac{R_{HH}(F) - R_{HH}(0)}{F} - \frac{R_{HH}(0) - R_{HH}(-F)}{F}\right) \Big/ -4\pi^2 R_{HH}(0)F \\
&= R_{HH}(F) + R_{HH}(-F) - 2\times R_{HH}(0) \Big/ -4\pi^2 R_{HH}(0)F^2 \\
&= 2\,\mathrm{Re}\{R_{HH}(F)\} - 2\times R_{HH}(0) \Big/ -4\pi^2 R_{HH}(0)F^2 \\
&= \frac{1 - \dfrac{\mathrm{Re}\{R_{HH}(F)\}}{R_{HH}(0)}}{2\pi^2 F^2}
\end{aligned} \quad . \qquad (2.25)$$

And the approximation of (2.23) is similar to the 2nd moment, the only difference is the m_1 phase shift, which is $R_{HH1}(f) = R_{HH}(f)\times e^{j2\pi f m_1}$. And the approximation of (2.23) is

$$\begin{aligned}
\hat{m}_{2,centre} &= 2\,\mathrm{Re}\{R_{HH1}(F)\} - 2\times R_{HH1}(0) \Big/ -4\pi^2 R_{HH1}(0)F^2 \\
&= \frac{1 - \dfrac{\mathrm{Re}\{R_{HH}(F)\}}{R_{HH}(0)}\times\cos\left(-\dfrac{\mathrm{Im}\{R_{HH}(F)\}}{R_{HH}(0)}\right) + \dfrac{\mathrm{Im}\{R_{HH}(F)\}}{R_{HH}(0)}\sin\left(-\dfrac{\mathrm{Im}\{R_{HH}(F)\}}{R_{HH}(0)}\right)}{2\pi^2 F^2}
\end{aligned} \quad . (2.26)$$

2.4.2 The Discrete Form of the Moments

Because all simulations are executed in discrete, it's necessary to transform m_1, m_2, and $m_{2,centre}$ into discrete form. We can assume that sampling frequency $F = 1/N$, where N is the FFT size, and the 1st moment in discrete and the 1st moment estimator in discrete is show as following equations:

$$\begin{cases} m_{n,1} = \dfrac{\sum_{l=0}^{L-1} \left| h_{[n,l]} \right|^2 l}{\sum_{l=0}^{L-1} \left| h_{[n,l]} \right|^2} \\ \hat{m}_{n,1} = \dfrac{-NR_{n,1,i}}{2\pi R_{n,0}} \end{cases} \tag{2.27}$$

denote that $m_{n,1}$ is the 1st moment, $\hat{m}_{n,1}$ is the 1st moment estimator,

$R_{n,k,r} = \mathrm{Re}\left\{ R_{n,HH}(kF) \right\}$, $R_{n,k,i} = \mathrm{Im}\left\{ R_{n,HH}(kF) \right\}$,and n is the n-th OFDM symbol. And the equations of the 2nd moment and the 2nd moment estimator in discrete are as follow

$$\begin{cases} m_{n,2} = \dfrac{\sum_{l=1}^{L-1} \left| h_{[n,l]} \right|^2 l^2}{\sum_{l=1}^{L-1} \left| h_{[n,l]} \right|^2} & (2.28a) \\ \hat{m}_{n,2} = N^2 \times \dfrac{1 - \dfrac{R_{n,1,r}}{R_{n,0}}}{2\pi^2} & (2.28b) \end{cases}$$

.

And the equations of the 2nd centre moment and the 2nd centre moment estimator in discrete are as follow

$$\begin{cases} m_{n,2,centre} = \dfrac{\sum_{l=0}^{L-1} \left| h_{1[n,l]} \right|^2 l^2}{\sum_{l=0}^{L-1} \left| h_{1[n,l]} \right|^2} & (2.29a) \\ \hat{m}_{n,2,centre} = N^2 \times \dfrac{1 - \dfrac{R_{n,1,r}}{R_{n,0}} \times \cos\left(\dfrac{R_{n,1,i}}{R_{n,0}} \right) + \dfrac{R_{n,1,i}}{R_{n,0}} \sin\left(\dfrac{R_{n,1,i}}{R_{n,0}} \right)}{2\pi^2} & (2.29b) \end{cases}$$

2.4.3 The Effect of Down-Sampling to the Moments Estimators

In chapter 2.4.2, the F is defined as 1/N, which means all subcarrier information is obtained. In fact, a receiver gets information only on pilot subcarriers. The CFR on pilot subcarriers $\mathbf{H}_n^{\mathrm{P}}$ can regard as the down sampling of the CFR $\mathbf{H}_n$ with F_S down-sampling rate. Comparing the following two steps:

$$\mathbf{H}_n \xrightarrow{\substack{\text{downsampling}\\ \text{and}\\ \text{padding zeros}}} \mathbf{H}0_n^{\mathrm{P}} \xrightarrow{\text{autocorrelation}} \mathbf{R}p_n \tag{s1}$$

$$\mathbf{H}_n \xrightarrow{\text{autocorrelation}} \mathbf{R}_n \xrightarrow{\text{down sampled}} \mathbf{R}_n^{\mathrm{P}} \tag{s2}$$

where $Rp_n(m) = \frac{1}{N_p}\sum_{k=1}^{N_p} H_{[n,P(k)]}{}^{*} H_{[n,P(k)+m]}$ and $R_n^P(m) = \frac{1}{N}\sum_{k=1}^{N} H_{[n,k]}{}^{*} H_{[n,k+mF_S]}$.

In (s1), the pilot signals $\mathbf{H}_n^{\mathrm{P}}$ are acquired at receiver, and then we use those pilots to access the autocorrelations. But all the autocorrelations we mentioned before are defined as steps (s2). It's important to know what's different in those two steps. With reference to Fig. 2.15, the down-sampling effects to the CIR in time domain are shown clearly.

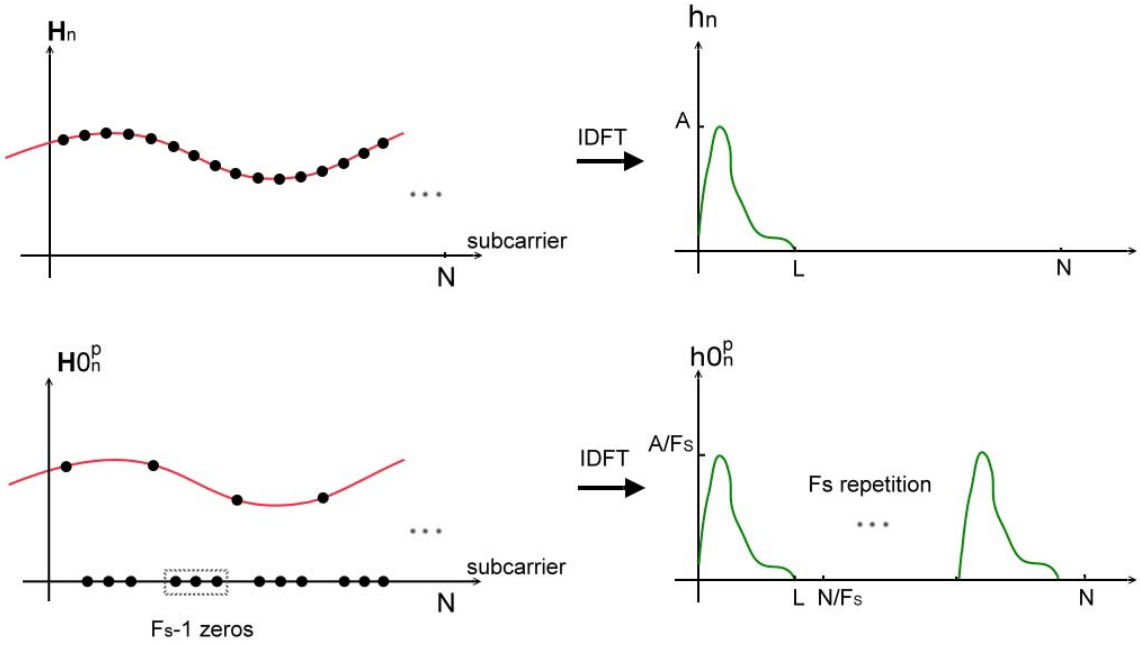

Fig. 2.15 Down Sampling Effects

And the differences in time domain of these two steps are shown in (2.30).

$$
\begin{array}{lllll}
\mathbf{H}_n & \xrightarrow{\substack{\text{downsampling}\\ \text{and}\\ \text{padding zeros}}} & \mathbf{H}0_n^{\mathrm{P}} & \xrightarrow{\text{autocorrelation}} & \mathbf{R}p_n \qquad \text{(s1)} \\
h_{[n,l]} & \rightarrow & h0_{[n,l]} & \rightarrow & \left|h0_{[n,l]}\right|^2 \\
\mathbf{H}_n & \xrightarrow{\text{autocorrelation}} & \mathbf{R}_n & \xrightarrow{\text{down sampled}} & \mathbf{R}_n^{\mathrm{P}} \qquad \text{(s2)} \\
h_{[n,l]} & \rightarrow & \left|h_{[n,l]}\right|^2 & \rightarrow & h3_{[n,l]}
\end{array}
\quad , \qquad (2.30)
$$

where $h1_{[n,l]} = \left|h0_{[n,l]}\right|^2$, $h2_{[n,l]} = \left|h_{[n,l]}\right|^2$, $h3_{[n,l]}$ is the F_S repetitions of l=1~N/F_S. We can see that if the channel length is shorter than N/F_S, and the $h3_{[n,l]}$ is equivalent to $h1_{[n,l]}$, and the moments estimator is usable. In other words, if the channel length is longer than N/F_S, there are aliasing in $h0_{[n,l]}$, and its autocorrelation $h1_{[n,l]}$ will not equal to $h3_{[n,l]}$, and the estimator is not work. With sapling theory, if the number of pilot subcarriers is not enough, the obtained information is unable to recover the original data, which means the N/FS will be shorter than the channel length.

2.4.4 The Relationships between Moments and Moments Estimator in Time Domain:

To evaluate the performance of an estimator, there is some background knowledge that needs to know. The relationship of the moments and the moment estimators in time domain can help with the analysis of the estimator performance. Therefore, we have to transform the frequency domain estimator to time domain to compare with the original moments.

The frequency response of channel is (1.3a):

$$H_{[n,k]} = \sum_{l=0}^{L-1} h_{[n,l]} W_N^{kl} \quad ,$$

where n is the n-th OFDM symbol. And the autocorrelation of $H_{[n,k]}$ is

$$R_n(m) = \tfrac{1}{N}\sum_{k=1}^{N} H_{[n,k]}{}^{*} H_{[n,k+m]}$$
$$= \tfrac{1}{N}\sum_{k=1}^{N}\sum_{l=0}^{L-1}\sum_{l_1=0}^{L-1} h^{*}_{[n,l]} e^{j\frac{2\pi kl}{N}} h_{[n,l_1]} e^{-j\frac{2\pi(k+m)l_1}{N}}$$
$$= \tfrac{1}{N}\sum_{k=1}^{N}\sum_{l=0}^{L-1}\sum_{l_1=0}^{L-1} h^{*}_{[n,l]} h_{[n,l_1]} e^{j\frac{2\pi kl-2\pi(k+m)l_1}{N}}$$

only when $l = l_1$, the elements of $R_n(m) \neq 0$, therefore

$$R_n(m) = \tfrac{1}{N}\sum_{k=1}^{N}\sum_{l=0}^{L-1} h^{*}_{[n,l]} h_{[n,l]} e^{j\frac{-2\pi ml}{N}}$$
$$= \sum_{l=0}^{L-1}\left|h_{[n,l]}\right|^2 e^{j\frac{-2\pi ml}{N}} \quad . \tag{2.31}$$
$$= \sum_{l=0}^{N-1}\left|h_{[n,l]}\right|^2 e^{j\frac{-2\pi ml}{N}}$$

Denote that the length of CIR is still L, but the value of $h_{[n,l]}$ from L~N-1 is zero. The reason to use N instead of L is that it's convenient to combine the effect of down sampling to the estimators. Use (2.31) to the estimators, the autocorrelation, (2.27b) and (2.28b), can be expressed in time domain as follow:

$$R_{n,1,r} = \mathrm{Re}\{R_n(F_S)\} = \sum_{l=0}^{N-1}\left|h_{[n,l]}\right|^2 \cos\left(\frac{2F_S\pi l}{N}\right)$$
$$R_{n,1,i} = \mathrm{Im}\{R_n(F_S)\} = -\sum_{l=0}^{N-1}\left|h_{[n,l]}\right|^2 \sin\left(\frac{2F_S\pi l}{N}\right) \tag{2.32}$$

And the 1st moment estimator of n-th symbol $\hat{m}_{n,1}$, (2.27b), is expressed as follows:

$$\hat{m}_{n,1} = -\frac{N\times R_{n,1,i}}{2\pi R_{n,0}} = \frac{N\sum_{l=0}^{N-1}\left|h_{[n,l]}\right|^2 \sin\left(\frac{2F_S\pi l}{N}\right)}{2\pi\sum_{l=0}^{N-1}\left|h_{[n,l]}\right|^2} \tag{2.33}$$

And the 2nd moment estimator of n-th symbol $\hat{m}_{n,2}$ is,

$$\hat{m}_{n,2} = N^2\frac{1-\frac{R_{n,1,r}}{R_{n,0}}}{2\pi^2} = \frac{N^2}{2\pi^2\sum_{l=0}^{N-1}\left|h_{[n,l]}\right|^2}\left(\sum_{l=0}^{N-1}\left(1-\cos\left(\frac{2F_S\pi l}{N}\right)\right)\left|h_{[n,l]}\right|^2\right) \tag{2.34}$$

If we use the plots to tell the difference between $\widehat{m_1}$ and m_1, we can see that the

summation path of m1 is linear and the summation path of $\widehat{m_1}$ is a sine wave. Fig 2.16 shows the summation paths of the 1st moment estimator and the1st moment. The left one is the summation path of the estimator, the right one is the summation path of the original moment, and the blue one is the CIR. Denote that the F_S equal to F, which means all subcarrier information is obtained, and there is no down sampling effects in Fig. 2.16:

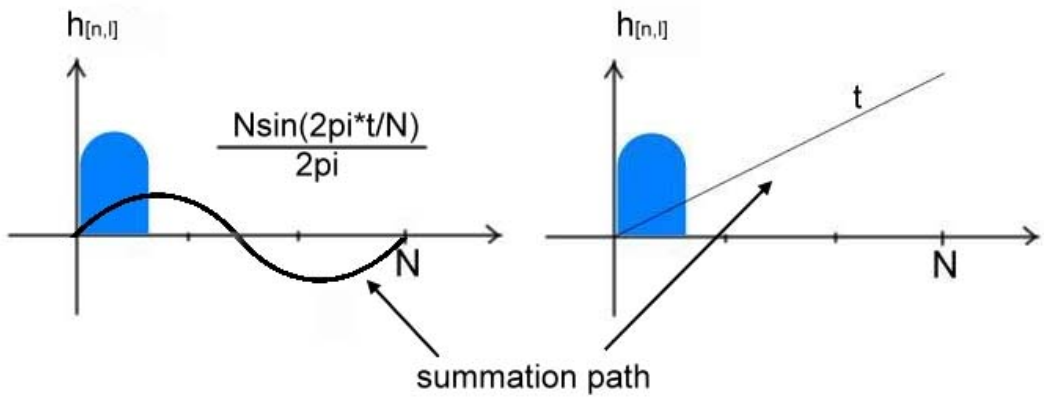

Fig. 2.16 The Summation Paths of the 1st Moment and its Estimator

From Fig. 2.16, (2.27a), and (2.33), we can know that the slope of summation paths is almost equivalent at the beginning paths, which is about N/4 paths. It tells that if the CIR is centered on first few paths, the estimator will be very accurate.

When it comes to the performance of the 2nd moment and the 2nd centre moment, there is a simplification has to do to the estimator, thus we can see the relations more clear. The following equation is the relation between m_2 and $m_{2,centre}$ in statistic.

$$E\left\{m_{2,centre}\right\} = E\left\{\left(x - E\left(x\right)\right)^2\right\} = E\left\{x^2\right\} - \left(E\left\{x\right\}\right)^2,$$

where x is the CIR. The simplification is: Assume that m_1 is perfectly estimated, which $E\{x\}= m_1$, and then $E\{x^2\}=m_2$ is the only parameter that affects the performance of the 2nd centre moment estimator. After this simplification, the performance evaluation of the 2nd centre moment cares only about the 2nd moment but not the complicated 2nd centre moment. As the 1st moment estimator does, the 2nd moment estimator also compares with the

original moment in time domain, and their summation paths are shown in Fig. 2.17. The cosine line is the summation path of the estimator, and the red line is the summation path of the original moment. Denote that F_S=F , which is same as the figure of 1st moments.

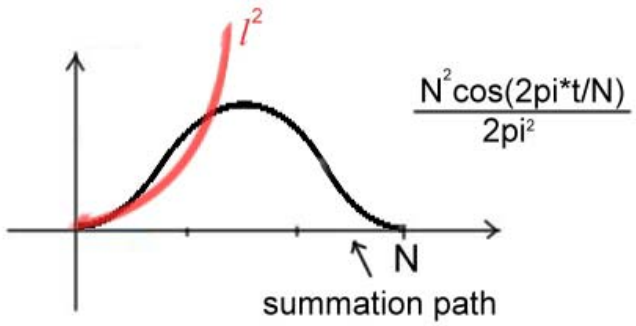

Fig. 2.17 The Summation Paths of the 2nd Moment and its Estimator

From the upper figure, we can see that the summation path of the estimator is almost equivalent to the one of the original moment before N/3 paths. It means that if the CIR is longer than N/3 paths, then the 2nd moment estimator will be failed.

It is assumed that all subcarrier information is obtained in upper two figures, however, often the F_S does not equal to F, and the summation paths also have some changes. These changes are effect from down sampling, which is discussed in Chapter 2.4.3. The summation path of first moments with down sampling effects is show in Fig. 2.18, and the red line is the summation path of m_1,and the black sin waves is the summation path of $\widehat{m_1}$, we may consider to adjust the amplitude of sine wave to gain a more accurate estimator with comparison to m_1. With down sampling effects, the m_1 estimator equation has a little change, which is as follow

$$\hat{m}_{n,1} = -\frac{N \times R_{n,1,i}}{2\pi R_{n,0}} = \frac{N \sum_{l=0}^{N/F_S-1} \left|h0_{[n,l]}\right|^2 \sin\left(\frac{2F_S \pi l}{N}\right)}{2\pi F_S \sum_{l=0}^{N/F_S-1} \left|h0_{[n,l]}\right|^2}. \tag{2.35}$$

The summation length is reduced from N-1 to (N-1)/F_S because of the F_S repetitions in time domain, and the F_S in denominator is used to reduce the amplitude of sine wave.

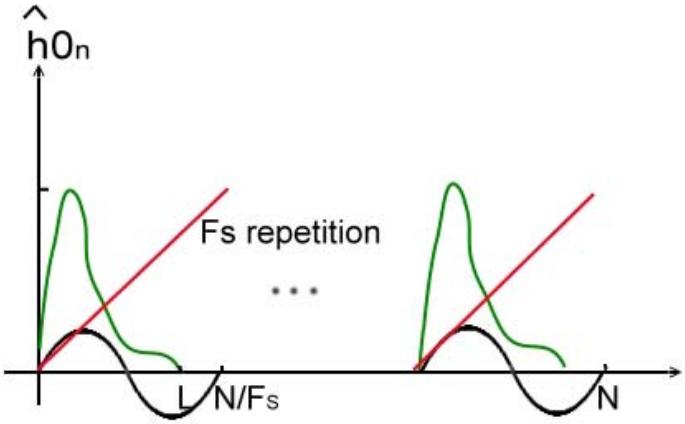

Fig. 2.18 The Summation Paths of m_1 with Down Sampling Effects

On the other hand,m2 estimator has the same down sampling effects as m1 estimator does. These effects are shown in Fig. 2.19. And the m2 estimator has the some changes too, which as follow:

$$\hat{m}_{n,2} = N^2 \frac{1-\frac{R_{n,1,r}}{R_{n,0}}}{2\pi^2} = \frac{N^2}{2\pi^2 F_S^{\,2} \sum_{l=0}^{N/F_S-1} \left|h0_{[n,l]}\right|^2} \left(\sum_{l=0}^{N/F_S-1} \left(1-\cos\left(\frac{2F_S \pi l}{N} \right) \right) \left|h0_{[n,l]}\right|^2 \right) \tag{2.36}$$

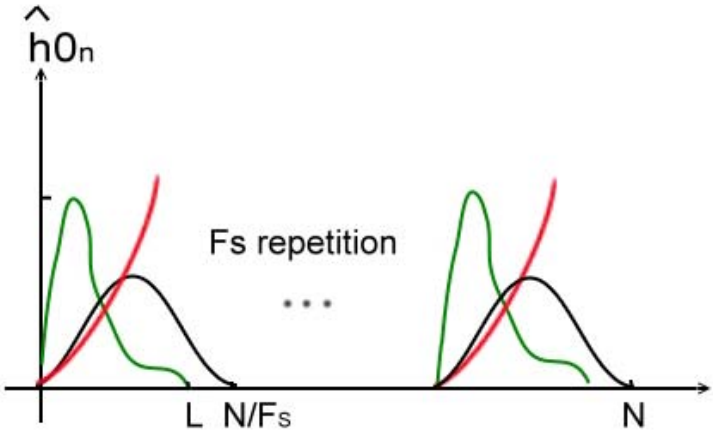

Fig. 2.19 The Summation Paths of m2 with Down Sampling Effects

And (2.35) and (2.36) are the equations used to evaluate the estimator performance in next section.

2.4.5 Improve the Accuracy of the Estimators

In Fig. 2.18 and Fig. 2.19, besides the CIR, which is not a controllable parameter at

the receiver, we can see that the amplitude of sine wave and cosine wave is the key to the accuracy performance. If we can slightly adjust the amplitude of sine and cosine wave based on the channel power delay profile, it would be a good solution to improve the accuracy of these estimators. To adjust the amplitude, the factor x and y is added into the denominator of m_1 and m_2 estimators respectively, and the estimators can rewrite as:

$$\hat{m}_{n,1} = -\frac{N \times R_{n,1,i}}{2\pi x R_{n,0}} = \frac{N \sum_{l=0}^{N/F_S-1} \left|h0_{[n,l]}\right|^2 \sin\left(\frac{2F_S \pi l}{N}\right)}{2\pi F_S x \sum_{l=0}^{N/F_S-1} \left|h0_{[n,l]}\right|^2}$$

$$\hat{m}_{n,2} = N^2 \frac{1-\frac{R_{n,1,r}}{R_{n,0}}}{2\pi^2 y} = \frac{N^2}{2\pi^2 F_S{}^2 y \sum_{l=0}^{N/F_S-1} \left|h0_{[n,l]}\right|^2} \left(\sum_{l=0}^{N/F_S-1} \left(1-\cos\left(\frac{2F_S \pi l}{N}\right)\right) \left|h0_{[n,l]}\right|^2 \right) \quad . \qquad (2.37)$$

Use the method of MMSE to find out the optimal x, the procedures are as eq. 2.38, and it is assumed that the total power is constant, which $\sum_{l=0}^{N/F_S-1} \left|h0_{[n,l]}\right|^2$ = constant B

$$\begin{aligned}
&\hat{m}_{n,1} - m_{n,1} \\
&= \frac{N \sum_{l=0}^{N/F_S-1} \left|h0_{[n,l]}\right|^2 \sin\left(\frac{2F_S \pi l}{N}\right)}{2\pi F_S x \sum_{l=0}^{N/F_S-1} \left|h0_{[n,l]}\right|^2} - \frac{\sum_{l=0}^{N/F_S-1} \left|h0_{[n,l]}\right|^2 l}{\sum_{l=0}^{N/F_S-1} \left|h0_{[n,l]}\right|^2} \\
&= \frac{1}{\sum_{l=0}^{N/F_S-1} \left|h0_{[n,l]}\right|^2} \left(\frac{N}{2\pi F_S x} \sum_{l=0}^{N/F_S-1} \left|h0_{[n,l]}\right|^2 \sin\left(\frac{2F_S \pi l}{N}\right) - \sum_{l=0}^{N/F_S-1} \left|h0_{[n,l]}\right|^2 l \right) \\
&= \frac{1}{B} \left(\frac{N}{2\pi F_S x} \sum_{l=0}^{N/F_S-1} \left|h0_{[n,l]}\right|^2 \sin\left(\frac{2F_S \pi l}{N}\right) - \sum_{l=0}^{N/F_S-1} \left|h0_{[n,l]}\right|^2 l \right)
\end{aligned} \quad . \qquad (2.38)$$

Because the summation range is N/F_S, where $\left|h0_{[n,l]}\right| = \left|h_{[n,l]}\right|$, eq. 2.38 can write as:

$$\hat{m}_{n,1} - m_{n,1} = \frac{1}{B} \left(\frac{N}{2\pi F_S x} \sum_{l=0}^{N/F_S-1} \left|h_{[n,l]}\right|^2 \sin\left(\frac{2F_S \pi l}{N}\right) - \sum_{l=0}^{N/F_S-1} \left|h_{[n,l]}\right|^2 l \right)$$

And the MSE and BIAS of the 1st moment estimator are:

$$\text{MSE:} E\left\{\left|\hat{m}_{n,1} - m_{n,1}\right|^2\right\} = \frac{1}{B^2} E\left\{\left| \sum_{l=0}^{N/F_S-1} \left(l - \frac{N}{2\pi F_S x} \sin\left(\frac{2F_S \pi l}{N}\right)\right) \times \left|h_{[n,l]}\right|^2 \right|^2\right\}$$

$$\text{BIAS: } E\left\{\hat{m}_{n,1}\right\} - E\left\{m_{n,1}\right\} = \frac{1}{B} E\left\{ \sum_{l=0}^{N/F_S-1} \left(l - \frac{N}{2\pi F_S x} \sin\left(\frac{2F_S \pi l}{N} \right) \right) \times \left| h_{[n,l]} \right|^2 \right\}$$

Assume that $h_{[n,l]}$~complex normal distribution $N(0,\sigma_l^{\,2})$, then the probability density function (PDF) of $\left|h_{[n,l]}\right|$ is Rayleigh distribution $R(\sigma_l\sqrt{\frac{\pi}{2}}, 2\sigma_l^{\,2})$, where R(a, b): a=E{x}, b= E{x^2}, and $E\{x^4\} = 12\sigma^4$, and the MSE and BIAS will be:

$$\text{MSE: } \frac{1}{B^2} \sum_{l=0}^{N/F_S-1} \left(l^2 - \frac{N}{\pi F_S x} l \sin\left(\frac{2\pi F_S l}{N} \right) + \frac{N^2}{4\pi^2 F_S^{\,2} x^2} \sin^2\left(\frac{2\pi F_S l}{N} \right) \right) \times 12\sigma_l^{\,4}$$

$$\text{BIAS: } \frac{1}{B} \sum_{l=0}^{N/F_S-1} \left(l - \frac{N}{2\pi F_S x} \sin\left(\frac{2F_S \pi l}{N} \right) \right) \times 2\sigma_l^{\,2}$$

We can see that MSE function is also a function of factor x:

$$f(x) = \sum_{l=0}^{N/F_S-1} \left(l^2 - \frac{N}{\pi F_S x} l \sin\left(\frac{2\pi F_S l}{N} \right) + \frac{N^2}{4\pi^2 F_S^{\,2} x^2} \sin^2\left(\frac{2\pi F_S l}{N} \right) \right) \times 12\sigma_l^{\,4}$$

Then the differential to x of f(x) is

$$\frac{df(x)}{dx} = \sum_{l=0}^{N/F_S-1} \left(\frac{N}{\pi F_S x^2} l \sin\left(\frac{2\pi F_S l}{N} \right) - \frac{N^2}{2\pi^2 F_S^{\,2} x^3} \sin^2\left(\frac{2\pi F_S l}{N} \right) \right) \times 12\sigma_l^{\,4} = 0$$

The f(x) will be minimized when x equals to

$$x_{MMSE} = \frac{N}{2\pi F_S} \frac{\sum_{l=1}^{N/F_S-1} \sigma_l^{\,4} \sin^2\left(\frac{2\pi F_S l}{N} \right)}{\sum_{l=1}^{N/F_S-1} \sigma_l^{\,4} l \sin\left(\frac{2\pi F_S l}{N} \right)}$$

And the m_1 estimator with factor x is

$$\hat{m}_{n,1,MMSE} = \frac{-NR_{n,1,i}}{2\pi x_{MMSE} R_{n,0}}$$

And the MMSE and the BIAS with MMSE factor x are:

$$\text{MMSE}: \frac{12}{B^2}\left[\sum_{l=0}^{N/F_S-1}\sigma_l^{\,4} l^2 - \frac{\left(\sum_{l=0}^{N/F_S-1}\sigma_l^{\,4} l \sin\left(\frac{2\pi F_S l}{N}\right)\right)^2}{\sum_{l=0}^{N/F_S-1}\sigma_l^{\,4}\sin^2\left(\frac{2\pi F_S l}{N}\right)}\right]$$

$$\text{BIAS with x: } \frac{2}{B}\left[\sum_{l=0}^{N/F_S-1}\sigma_l^{\,2} l - \frac{\left(\sum_{l=0}^{N/F_S-1}\sigma_l^{\,2}\sin\left(\frac{2F_S\pi l}{N}\right)\right)\left(\sum_{l=1}^{N/F_S-1}\sigma_l^{\,4} l \sin\left(\frac{2\pi F_S l}{N}\right)\right)}{\sum_{l=1}^{N/F_S-1}\sigma_l^{\,4}\sin^2\left(\frac{2\pi F_S l}{N}\right)}\right]$$

It's obviously that m_1 is a biased estimator. After evaluated m1 estimator, we use the same method to find out the y factor of the 2nd moment, the MSE and BIAS of m_2 estimator are:

$$\text{MSE:} E\left\{\left|\hat{m}_{n,2} - m_{n,2}\right|^2\right\} = \frac{1}{B^2} E\left\{\left|\sum_{l=0}^{N/F_S-1}\left(\frac{N^2\left(1-\cos\left(\frac{2F_S\pi l}{N}\right)\right)}{2\pi^2 F_S y} - l^2\right)\times\left|h_{[n,l]}\right|^2\right|^2\right\}$$

$$\text{BIAS: } E\left\{\hat{m}_{n,2}\right\} - E\left\{m_{n,2}\right\} = \frac{1}{B} E\left\{\sum_{l=0}^{N/F_S-1}\left(\frac{N^2\left(1-\cos\left(\frac{2F_S\pi l}{N}\right)\right)}{2\pi^2 F_S y} - l^2\right)\times\left|h_{[n,l]}\right|^2\right\}$$

The definition of channel is as same as m_1, $\left|h_{[n,l]}\right|$ is Rayleigh distribution $R(\sigma_l\sqrt{\frac{\pi}{2}}, 2\sigma_l^{\,2})$.

And MSE and BIAS become:

$$\text{MSE: } \frac{1}{B^2}\sum_{l=0}^{N/F_S-1}\left(\frac{N^2\left(1-\cos\left(\frac{2F_S\pi l}{N}\right)\right)}{2\pi^2 F_S y} - l^2\right)^2 \times 12\sigma^4$$

$$\text{BIAS: } E\left\{\hat{m}_{n,2}\right\} - E\left\{m_{n,2}\right\} = \frac{1}{B}\sum_{l=0}^{N/F_S-1}\left(\frac{N^2\left(1-\cos\left(\frac{2F_S\pi l}{N}\right)\right)}{2\pi^2 F_S y} - l^2\right)\times 2\sigma^2$$

And let f(y) =MSE, and when df(y)/dy=0, and y is the MMSE factor, which is

$$y_{MMSE} = \frac{N^2}{2\pi^2 F_S^{\,2}} \frac{\sum_{l=1}^{N/F_S-1} \sigma_l^{\,4} \left(1-\cos\left(\frac{2\pi F_S l}{N}\right)\right)^2}{\sum_{l=1}^{N/F_S-1} \sigma_l^{\,4} l^2 \left(1-\cos\left(\frac{2\pi F_S l}{N}\right)\right)}$$

And $m_{n,2,centre}$ and $m_{n,2}$ estimators with factor y can write as:

$$\hat{m}_{n,2,centre} = N^2 \times \frac{1-\frac{R_{n,1,r}}{R_{n,0}} \times \cos\left(\frac{R_{n,1,i}}{R_{n,0}}\right) + \frac{R_{n,1,i}}{R_{n,0}} \sin\left(\frac{R_{n,1,i}}{R_{n,0}}\right)}{2\pi^2 F_S^{\,2} y_{MMSE}}$$

$$\hat{m}_{n,2} = N^2 \frac{1-\frac{R_{n,1,r}}{R_{n,0}}}{2\pi^2 F_S^{\,2} y_{MMSE}}$$

And MMSE of m_2 and BIAS of m_2 with factor y are:

$$\text{MMSE: } \frac{12}{B^2}\left(\sum_{l=0}^{N/F_S-1} l^4 \sigma_l^{\,4} - \frac{\left(\sum_{l=0}^{N/F_S-1} l^2 \left(1-\cos\left(\frac{2F_S \pi l}{N}\right)\right)\sigma_l^{\,4}\right)^2}{\sum_{l=0}^{N/F_S-1} \left(1-\cos\left(\frac{2F_S \pi l}{N}\right)\right)^2 \sigma_l^{\,4}}\right)$$

$$\text{BIAS: } \frac{2}{B}\sum_{l=0}^{N/F_S-1}\left(\frac{N^2\left(1-\cos\left(\frac{2F_S \pi l}{N}\right)\right)}{2\pi^2 F_S y} - l^2\right) \times 2\sigma^2$$

Chapter 3

Pilot-Aided Channel Estimation for MIMO-OFDM

3.1 Reasons to extend SISO-OFDM to MIMO-OFDM

Extending SISO-OFDM to MIMO-OFDM aims to provide spatial diversity gains by multi-antenna. The multi-antenna technique is a popular method, and there are many new algorithms designed to fully utilize its tremendous potential. Channel estimation for MIMO systems is important; the algorithm proposed in Chapter2 is designed based on SISO-OFDM, and if we want to use the MA-LPIFA method in MIMO-OFDM system without changing the algorithm, the architecture of MIMO-OFDM must be considered. In this chapter the Alamouti scheme and MA-LPIFA are combined to provide an effective channel estimation method for MIMO-OFDM.

3.2 The Architecture of the MIMO-OFDM

To adapt those pilot interpolation methods in MIMO without changing the interpolation algorithms, the pilot interpolation must be completed in single channel information, which means there is a space decoder block needed to separate the multi-input for each receiver. Fig. 3.1 shows the idea of the architecture of MIMO-OFDM with comb-type pilot inserted, noted that the architecture after the spatial decoder is as same as the single channel estimation.

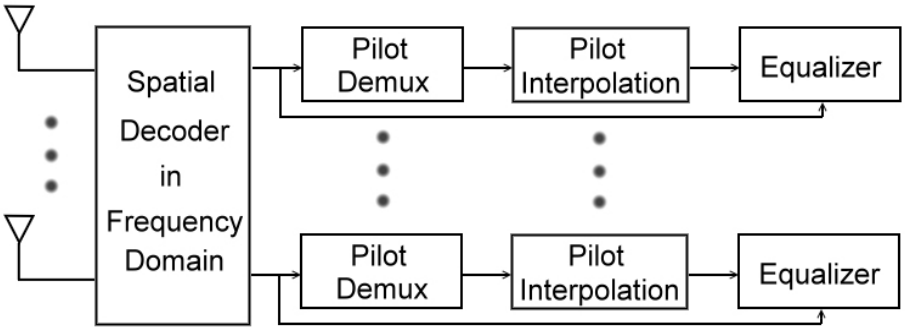

Fig. 3.1 The Architecture of the MIMO-OFDM Channel Estimation in Current Idea

3.3 The Space-Time CODEC for MIMO-OFDM

The Space-Time codes are exploited to extract the relations between different antennas; one of the famous S-T code schemes is Alamouti scheme [12]. In this these, the Alamouti scheme is the only method we use to extract the multi-antenna equations. In Alamouti scheme, the antennas are design as 2 transmitters and M receiver, which is 2M diversity. The encoding and transmission sequence for the two-branch transmit diversity scheme is shown in table2.

	Antenna0	**Antenna1**
Time t (n-th symbol)	S0	S1
Time t+T (n+1-th symbol)	-S1*	S0*

Table 2 The Encoding and Transmission Sequence for the Two-Branch Transmit Diversity Scheme

In Table2, S0 and S1 are denoted as the n-th transmitted symbol by antenna0 and antenna1 respectively, and * is the complex conjugate notation. In Fig. 3.2 is the channel model with 2*M diversity.

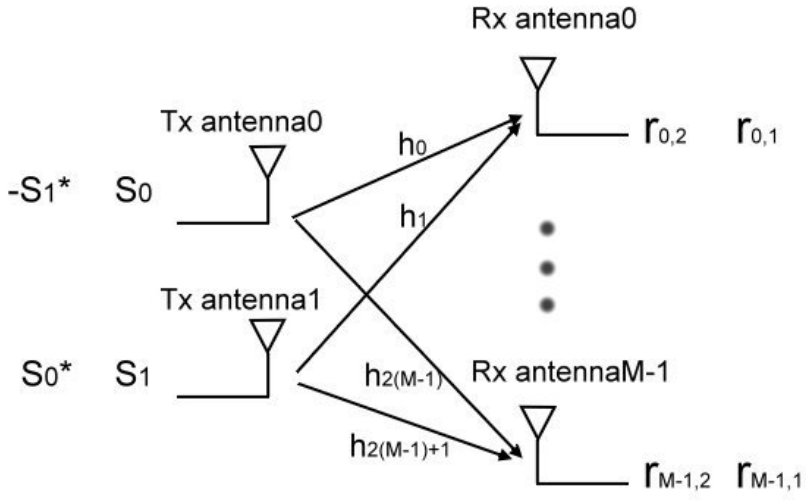

Fig. 3.2 The 2*M MIMO Channel Model

Denote that

$$\begin{cases} h_{2i} = \text{The channel of Tx antenna0 and Rx antenna } i \\ h_{2i+1} = \text{The channel of Tx antenna1 and Rx antenna } i \end{cases}$$

$$\begin{cases} n_{i,1} = \text{The noise of Tx antenna0 and Rx antenna } i \text{ at time t (the first symbol)} \\ n_{i,2} = \text{The noise of Tx antenna0 and Rx antenna } i \text{ at time t+T (the second symbol)} \end{cases}$$

$$\begin{cases} r_{i,1} = \text{The received signal at time t (the first symbol) of Rx antenna } i \\ r_{i,2} = \text{The received signal at time t+T (the second symbol) of Rx antenna } i \end{cases}$$

With the MIMO channel model, the received signal can expressed as follow

$$\begin{cases} r_{i,1} = h_{2i}s_0 + h_{2i+1}s_1 + n_{i,1} \\ r_{i,2} = -h_{2i}s_1^* + h_{2i+1}s_0^* + n_{i,2} \end{cases}. \tag{3.1}$$

Exploiting eq. 3.1, the channel information is accessible if the transmitted signal is known, which is as follow

$$\begin{cases} h_{2i} \approx \dfrac{r_{i,1}s_0^* - r_{i,2}s_1}{\left(|s_0|^2 + |s_1|^2\right)} \\ h_{2i+1} \approx \dfrac{r_{i,1}s_1^* + r_{i,2}s_0}{\left(|s_0|^2 + |s_1|^2\right)} \end{cases}.$$

In Alamouti scheme, the CIR is assumed not changed during time t to time t+T, which

means the first and the second symbol suffer the same channel effects. Because the pilot information is inserted in frequency domain, the Alamouti encoder and decoder are implemented in frequency domain. Fig. 3.3 is the block diagram of MIMO-OFDM with Alamouti scheme in detail.

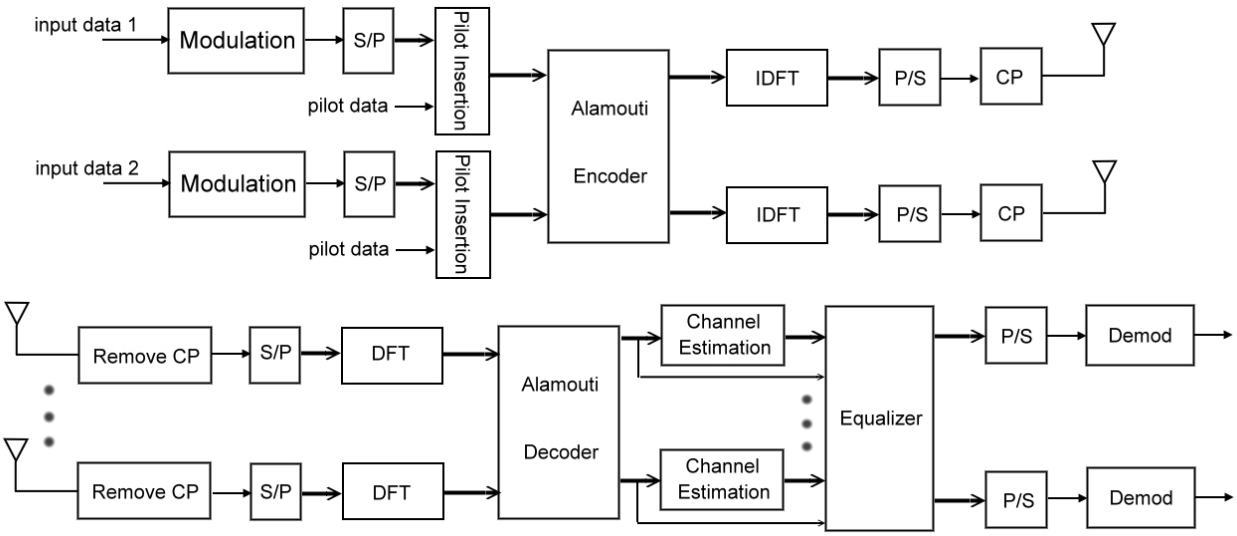

Fig. 3.3 The Block Diagram of MIMO-OFDM with Alamouti Scheme

3.4 How to Apply 1st and 2nd Moments in MIMO

With this MIMO-OFDM architecture, the complicated relationships of multi-antenna are solved by Alamouti CODEC and Alamouti equalizer blocks. After passing through Alamouti Decoder, each output stream can be regarded as a SISO-OFDM system. Therefore, all the channel estimation methods based on comb-type pilot interpolation in SISO-OFDM system are adaptable in MIMO-OFDM system without changing the algorithms. Since each output stream of Alamouti decoder represents each Tx-Rx path, the CFR information on pilot subcarrier is able to calculate the 1st and 2nd moments just as Chapter2 does.

Chapter 4

Simulation Results

4.1 Some Simulation Result of the Moment Estimators

The first series simulation results are the improvements of the 1st and 2nd moment estimator with factors x and y added. There are three types of power delay profiles (PDP) in this simulation, which are step function, exponential function, and normal function. Denote that the total powers of them are equal. In Fig. 4.1, there are three types of PDPs.

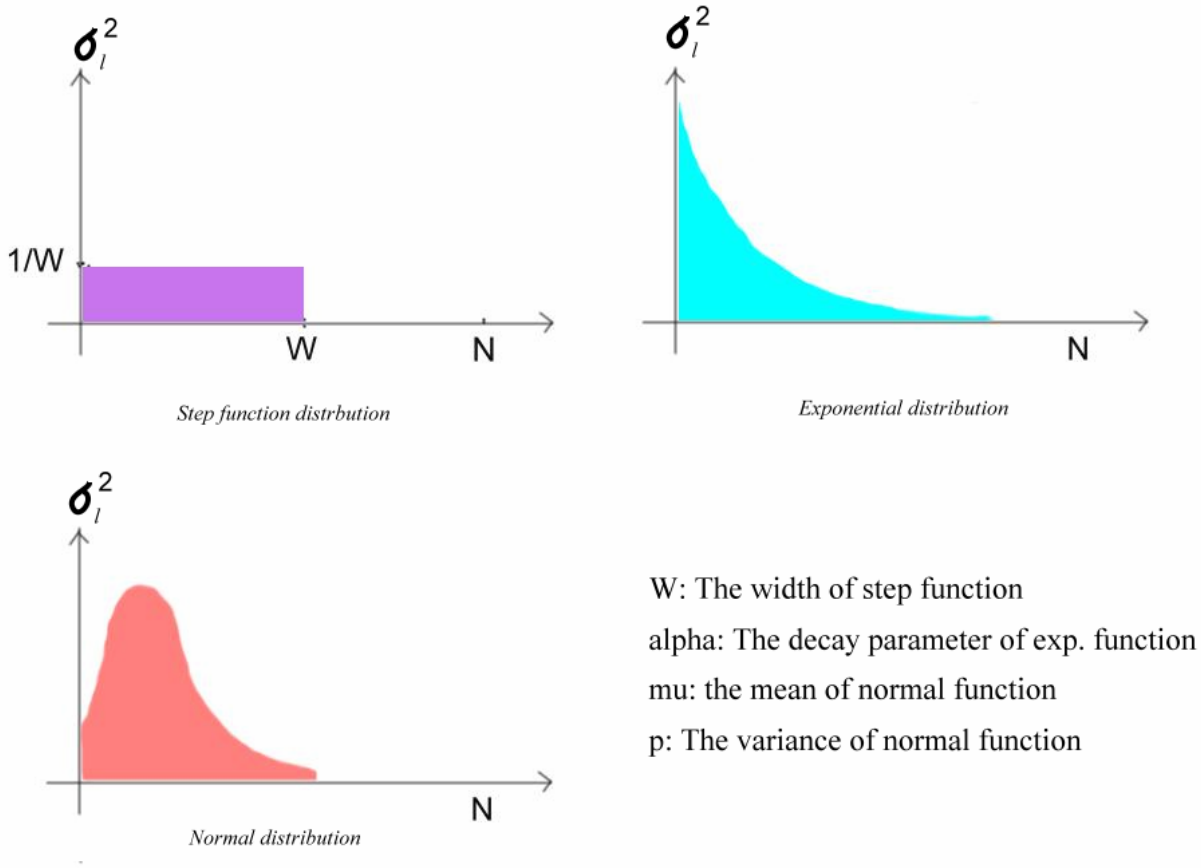

Fig. 4.1 Three Types of PDPs

In the simulation, the channel length N is 1000, pilot subcarrier number is 333, and all

PDP has the same power, which is equal to one. In Fig. 4.2 and Fig. 4.3, the x-axis of uniform distribution is the width of step function PDP, the x-axis of exponential distribution is the decay parameter alpha, where

$$\sigma_l^{\,2} = e^{-\text{alpha}\bullet l} \Big/ \int_{l=1}^{N} e^{-\text{alpha}\bullet l} dl\,,$$

The x-axis of normal distribution is the mean value mu, mu=1:200 p=50, and the x-axis of normal distribution1 is the variance value p, p=1:200 mu=50.

The normal distribution is

$$\sigma_l^{\,2} = e^{-\frac{(l-\text{mu})^2}{p^2}} \Big/ \text{normalizer}\sqrt{2\pi\bullet \text{p}^2}\,,$$

where $\text{normalizer} = \int_{l=1}^{l=N} e^{-\frac{(l-\text{mu})^2}{p^2}} \Big/ \sqrt{2\pi\bullet \text{p}^2}\, dl$

The y-axis in Fig. 4.2 and Fig. 4.3 are the normalized MSE of the estimators in db, which are

$$10\bullet\log_{10}\left(\frac{E\left\{\left|\hat{m}_1 - m_1\right|^2\right\}}{E\left\{m_1^{\,2}\right\}}\right) \text{ and } 10\bullet\log_{10}\left(\frac{E\left\{\left|\hat{m}_2 - m_2\right|^2\right\}}{E\left\{m_2^{\,2}\right\}}\right) \text{ respectively.}$$

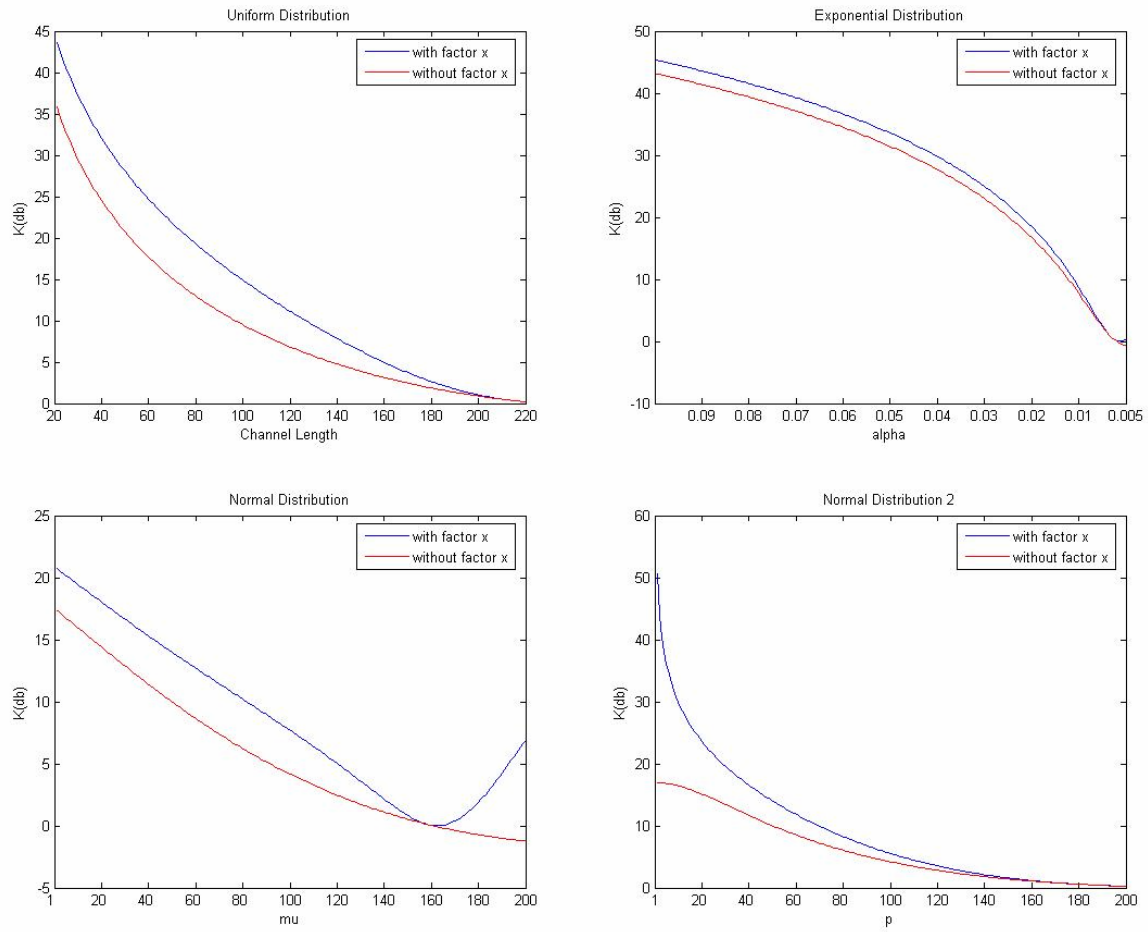

Fig. 4.2 The Normalized MSE of m1 Estimator

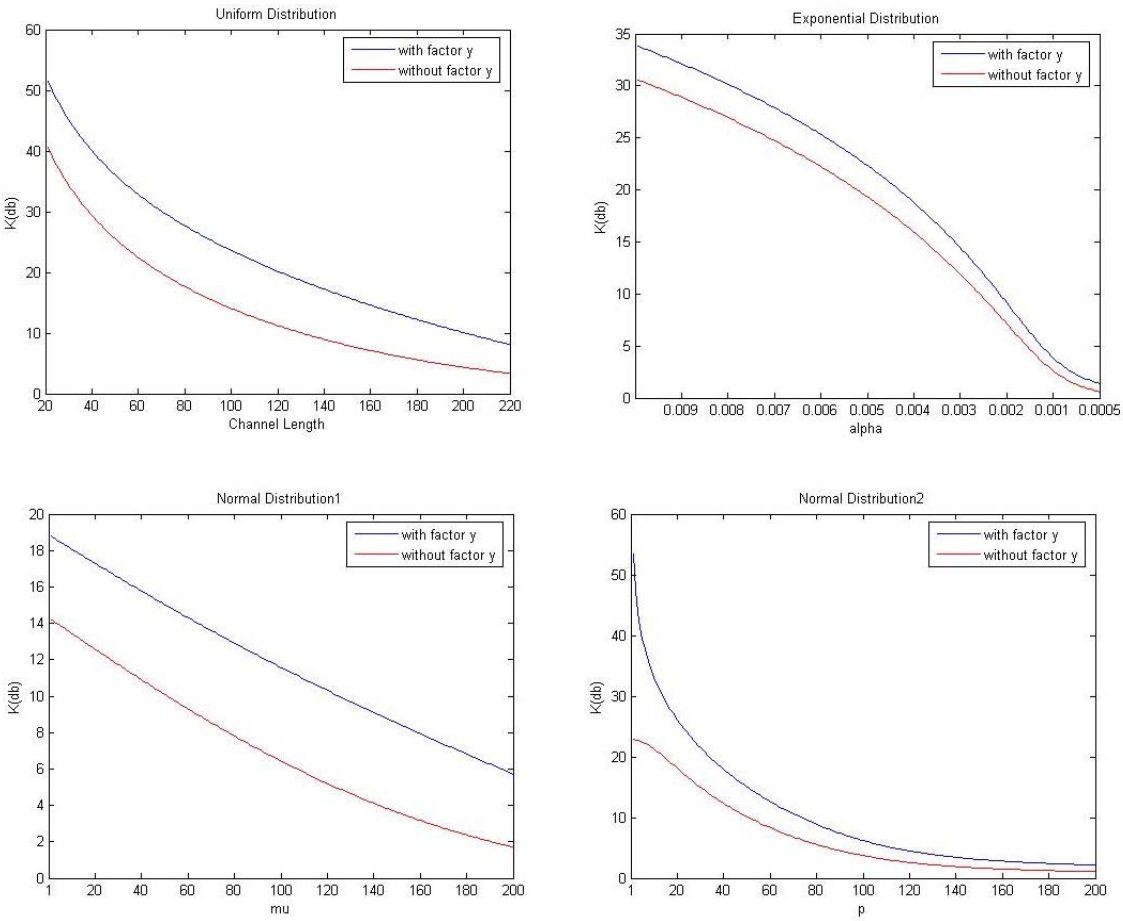

Fig. 4.3 The Normalized MSE of m2 Estimator

In Fig 4.2, the Normal Distribution1, the blue line with factor x get raised after mu >160. The reason is when aliasing occurred, the estimated m1 is negative, which is wrong. However, the x factor is negative too, and that is the reason the blue line get raised when mu>160. With respect to the summation paths of 1st moment, we can see that when PDP is shorter than $N/(4*F_S)$, the m1 estimator is reliable. In the simulation $N/(4*F_S) = 83$. And with respect to summation path of 2nd moment, the estimator is reliable when PDP is shorter than $N/(3*F_S)$, which is 111 in this simulation.

In Fig. 4.4 and Fig. 4.5 are the simulations of MSE of m1 and m2 respectively, which using the Monte Carlo method and theoretical value. The PDP in these two figures are the exponential distribution, and is the same as the normal distribution PDP in Fig. 4.2 and Fig. 4.3.

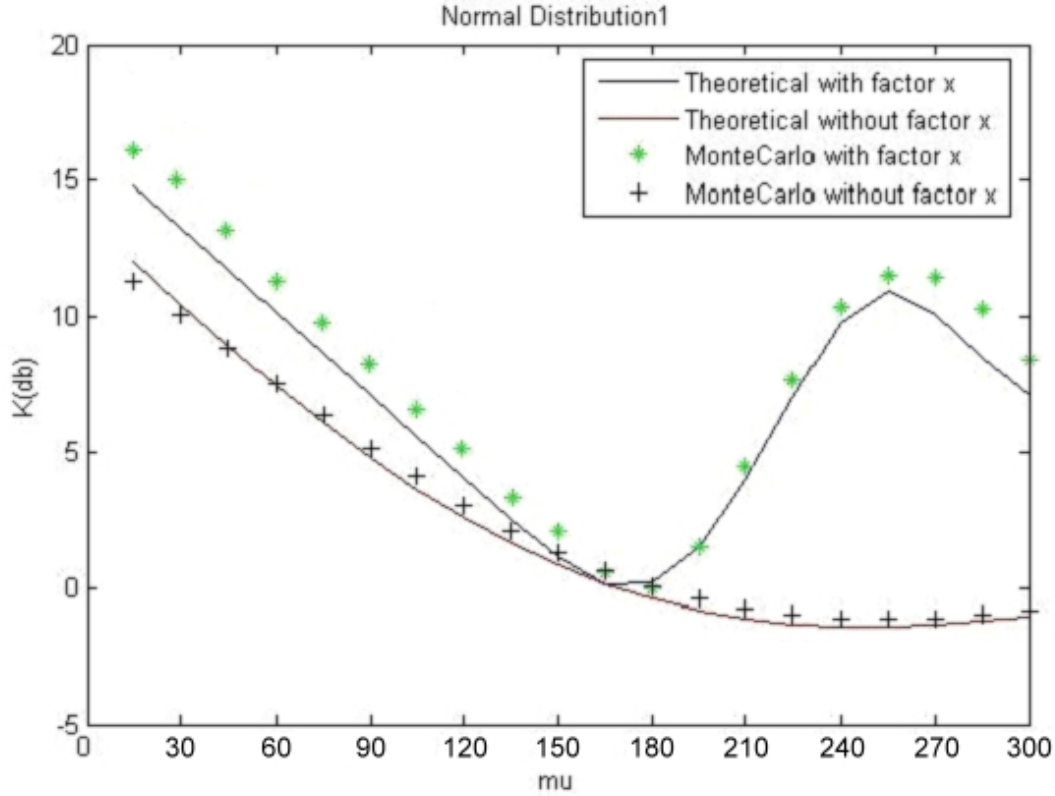

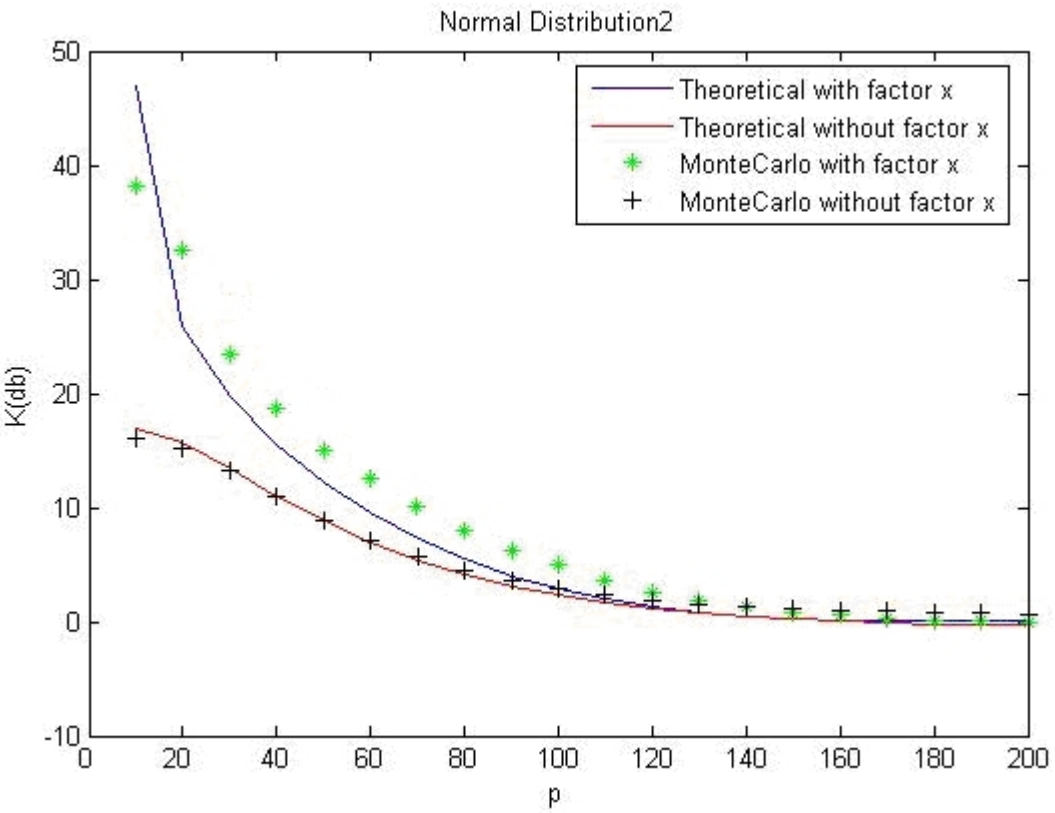

Fig. 4.4 The m1 Estimator MSE of Theoretical Value and Monte Carlo Method

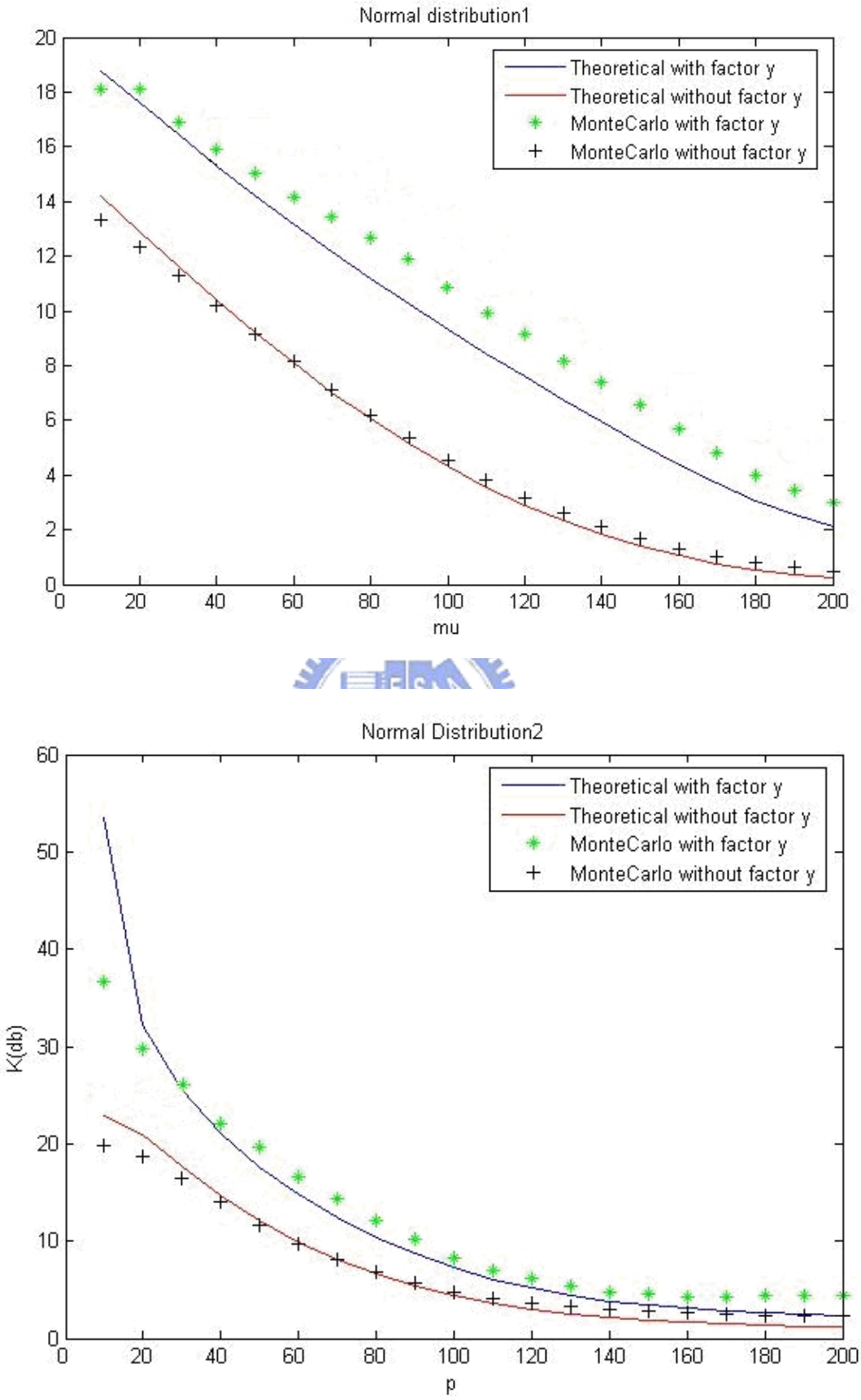

Fig. 4.5 The m2 Estimator MSE of Theoretical Value and Monte Carlo Method

4.2 Some Simulation Results of the MIMO-OFDM with the Interpolation methods

MIMO-OFDM system parameters used in the simulations are illustrated in **Table 3**. Since the aim is to observe channel estimation performance, it assumed to be perfect synchronization in the simulations. Moreover, the guard interval is assumed to be longer than the maximum delay spread of the channel.

Table 3 Simulation Parameters

Parameters	**Specifications**
FFT Size	1024
Pilot Ratio	1/11
Guard Interval	64
Antenna	2*2
Signal Constellation	QPSK
Channel Model	Rayleigh fading
Channel Length	20
Power Delay Profile	Exponential

The simulation shows the BER of different interpolation methods used in MIMO-OFDM in different SNR. The simulation result is shown in Fig.4.6. The X-axis represent SNR in db, and the noise is added after the signal convolution to CIR, and the noise power is expressed as

$$\text{noise power} = 10^{-\mathrm{SNR}/10} \times \frac{FFT_length + CP_length}{FFT_length}.$$

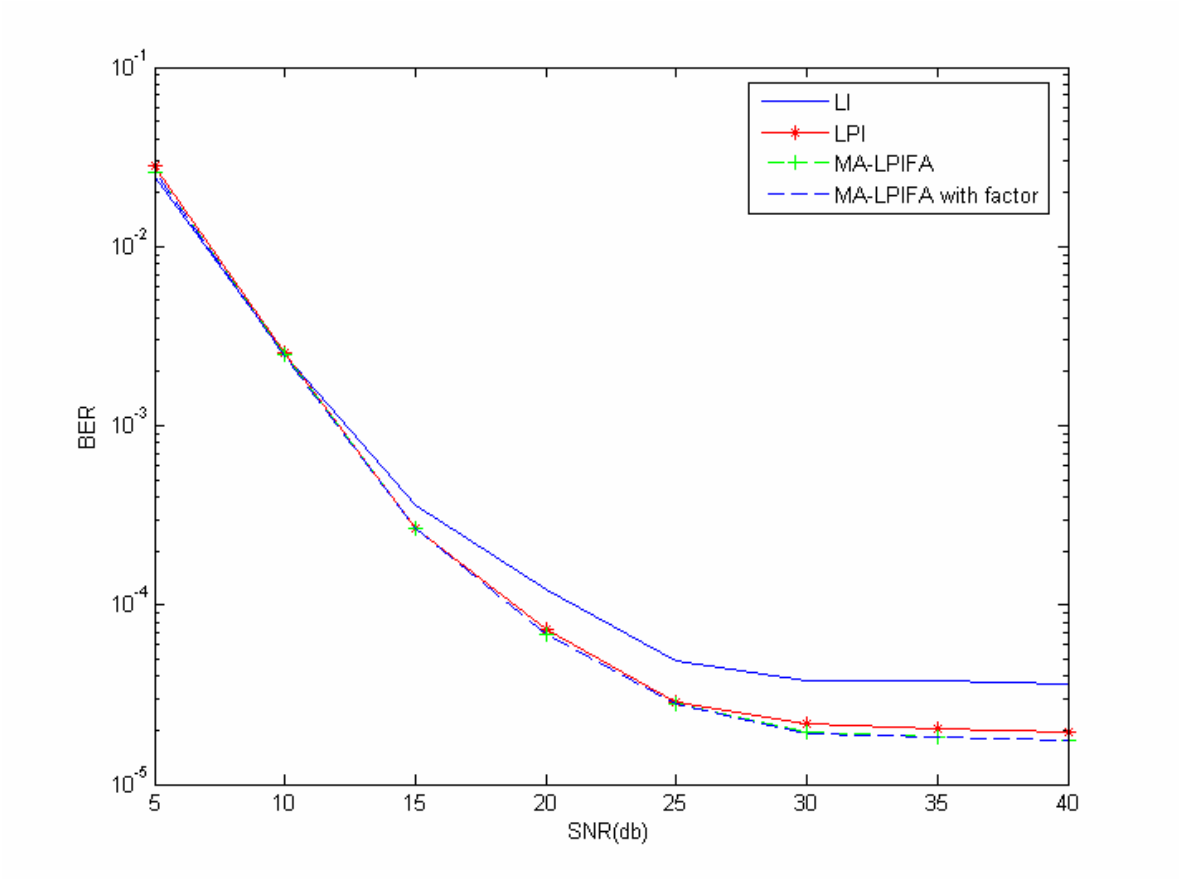

Fig. 4.6 BER Performance versus SNR for the Equalizer Based On Alamouti with Comb-Type Pilot Arrangements

Chapter 5
Conclusion

There are two contributions achieved in this thesis. First, a comb-type pilot aided channel estimation method (MA-LPIFD) is proposed. Second, the architecture of MIMO-OFDM that is able to apply to MA-LPIFD is designed. From the simulation result, we can see that the BER performance is better than traditional LPI, and the costs are N_P+3 multiplications and 2*N_P additions to access filter design indexes. Denote that N_P is the number of pilot subcarrier.

Besides the contributions, there are still some future works and some survey I haven't completed. First, in chapter2, if the centroid (first moment) of CIR can be replaced by the center of CIR, the center of the filter can be designed more precisely, and the performance of BER must be improved. I think the key point is to figure out the relations between time domain and frequency of the center of CIR. Second, at the first place, the Cramér-Rao Lower Bound (CRLB) of this MA-LPIFD method is my index to evaluate how good (or how bad) this estimator is. However, with some mathematical problems, for example, it is difficult to combine $\theta_{n,1} = \sum_{l=0}^{L-1} \left| h_{[n,l]} \right|^2 l \Big/ \sum_{l=0}^{L-1} \left| h_{[n,l]} \right|^2$ and $\hat{\theta}_{n,1} = N \sum_{l=0}^{N-1} \left| h_{[n,l]} \right|^2 \sin\left(\frac{2F_S \pi l}{N} \right) \Big/ 2\pi \sum_{l=0}^{N-1} \left| h_{[n,l]} \right|^2$ these two equations. The analysis of CRLB of this estimator is ceased. Third, in Chapter3, the drawback of this Alamouti-based MIMO-OFDM architecture is that it is assumed the CIR is unchanged in the period of two connecting symbols, and if the CIR changes faster than two symbol time, this architecture will be failed. I think there will be some architecture that can fix this

problem. Forth, in Chapter4, in the simulation, there are some improvement spaces in the usage of the 1st and 2nd moments. The filter design is not the topic of this thesis, but it is important when it comes to BER performance evaluation. If the moments can be used better, the filter will have better performance in filtering out the noise, and estimate the CFR more precisely.

References

[1] Juha Heiskala and John Terry, *OFDM Wireless LANs – A Theoretical and Practical Guide*. SAMS.

[2] Salzberg, B.R, "Performance of an Efficient Parallel Data Transmission System," *IEEE Trans. Comm.*, Vol. COM-15, pp.805-813, Dec. 1967.

[3] ESTI EN 300 744 V1.5.1, "Digital Video Broadcasting (DVB); Framing structure, Channel Coding and Modulation for Digital Terrestrial Television," Nov. 2004.

[4] IEEE 802.11a IEEE Standards for Wireless LAN Medium Access Control and Physical Layer Specifications, Nov. 1999.

[5] G. J. Foschini and M. J. Gans, "On limits of wireless communications in a fading environment when using multiple antennas,"*Wireless Personal Communication*, vol. 6, no. 3, pp. 311–335, Mar. 1998.

[6] Gordon L. Stuber, Steven W. McLaughlin, Mary Ann Ingram, "Broadband MIMO – OFDM Wireless Communication"

[7] Yushi Shen and Ed Martinez, "Channel Estimation in OFDM system," Freescale Semiconductor, A3059, 2006

[8] Zhongshan Wu, Jianqiang He, Guoxiang GU, "Design of Optimal Pilot-tones for Channel Estimation in MIMO-OFDM system," *IEEE Communications Society*.

[9] Günter, "Channel Estimation in Two Dimensional for OFDM Systems with Multiple Transmit Antennas," GLOBECOM, pp. 211-215, 2003.

[10] Edfors, O., Sandell, M., Van de Beek, J.-J., Landström, D., and Sjöberg, F., *An Introduction to Orthogonal Frequency Division Multiplexing*, Luleå, Sweden: Luleå Tekniska Universitet, 1996, pp. 1–58.

[11] The Reserved Resource

[12] S. M. Alamouti, “A simple transmit diversity technique for wireless communication,” *IEEE J. Sel. Areas Comm.*, 16(8), 1451-1458, Oct. 1998.